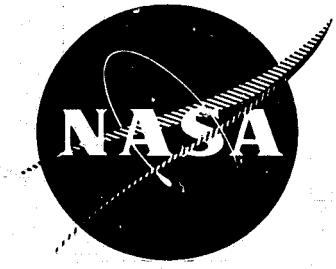

NASA CR 134520

EFFECTS OF PROCESSING ON THE CARRIER LIFETIME IN SILICON SOLAR CELLS

by P. A. Iles and S. I. Soclof

GLOBE - UNION INC.
Centralab Semiconductor
4501 N. Arden Drive
El Monte, California 91734

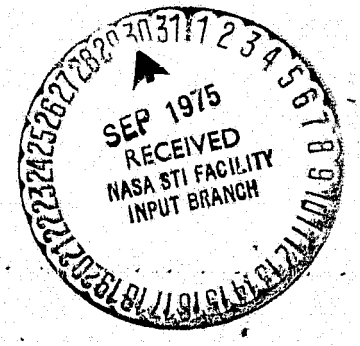

Prepared for

NATIONAL AERONAUTICS AND SPACE ADMINISTRATION

NASA Lewis Research Center

Contract NAS 3 - 15689

1. Report No.	2. Govt. Accession No.	3. Recipient's Catalog No.
NASA CR 134520		

4. Title and Subtitle	5. Report Date
EFFECTS OF PROCESSING ON THE CARRIER LIFETIME IN SILICON SOLAR CELLS.	February 1975
	6. Perf. Organisation Code.

7. Author(s).	8. Perf. Organisation Report#
P. A. Iles and S. I. Soclof	

9. Performing Organisation.	10. Work Unit No.
Globe - Union Inc. Centralab Semiconductor 4501 N. Arden Drive El Monte, California 91734	11. Contract or Grant No. NAS 3 - 15689

12. Sponsoring Agency.	13. Type of Report.
National Aeronautics and Space Admin. Lewis Research Center 21000 Brookpark Rd. Cleveland, Ohio 44135	Contractor Report
	14. Sponsoring Agency Code.

15. Supplementary Notes.

Project Manager, Henry W. Brandhorst, Jr. MS 302-1
NASA Lewis Research Center.
Cleveland, Ohio

16. Abstract.

This was a study of the effects of solar cell processing on the minority carrier lifetime in silicon. Measurments were made of the diffusion length and solar cell properties for ingots covering a wide range of doping and other ingot properties. The results showed that the cell processing did not cause appreciable change in diffusion length. The effects of heavy doping concentrations on solar cell performance were studied.

17. Key Words (Suggested by Author(s))	18. Distribution Statement.
Lifetime Silicon Solar Cells Process effects Ingot Variations	Unclassified - unlimited

19. Security Classif.	20. Security Classif. (page)	21. No. Pages	22. Price*
Unclassified	Unclassified	99	

* For sale by the Nat. Tech. Inf. Service, Springfield, Va. 22151

TABLE OF CONTENTS

TABLE OF CONTENTS (contd.)

LIST OF TABLES

LIST OF FIGURES

LIST OF FIGURES (contd.)

SUMMARY

This report describes measurements to determine the effects that solar cell processing steps have on the minority carrier lifetime in the silicon.

The experimental work included measurement of diffusion lengths of the silicon at various stages of cell fabrication, of solar cell properties, and of the PN junction properties. The measurements covered a wide range of resistivities (10 to 0.01 ohm-cm) and included combinations of extreme concentrations (high and low) of dislocations and oxygen.

The results showed that the major cell process steps did not usually cause appreciable change in diffusion lengths. The solar cell currents obtained supported the diffusion length measurements. Attempts were made to relate the voltage behavior of the cells with the diode properties and the properties of the ingots.

EFFECTS OF PROCESSING ON THE CARRIER LIFETIME IN SILICON SOLAR CELLS

1.0 INTRODUCTION

Silicon solar cells have received intensive development, and they have provided secondary power for most of the spacecraft flown to date. The requirements for space useage are demanding, requiring a combination of highest electrical output, light weight, and a good degree of resistance to damage caused by charged particles encountered in orbit. The silicon material providing the best combination of properties has been high quality, single crystal, P-type, around 1 to 10 ohm-cm, with a shallow N+ diffused layer.

There is still the possibility of obtaining increased output from silicon solar cells. A most promising area would be to obtain the higher voltages theoretically possible when lower resistivity silicon is used as the starting material for solar cells.[1-3]

In recent years there has been renewed interest in using solar cells to provide some earth surface power at levels sufficient to help the anticipated energy crisis. It is probable that in order to maintain costs sufficiently low, the silicon used will not be in single crystal form, and also may not fall in the resistivity range used most for space cells.

1.1 Objectives of the Present Study

This program studied solar cells made from silicon ingots deliberately doped to give a wide range of resistivity, particularly lower resistivities (below 1 ohm-cm).

The work used present cell processing methods and evaluated the effect of these methods on the minority carrier diffusion length (or lifetime) in the silicon ingots and on the properties of the solar cells made by applying all the process steps to this range of ingots.

1.1.1 Program Sequence

(a) To predetermined specifications, a number of special silicon ingots was obtained; these ingots spanned three decades of resistivity (0.01 to 10 ohm-cm). The group also included ingots which had the extreme values of two other important silicon crystal growth parameters, namely oxygen concentration and dislocation density.

(b) These special ingots were processed into solar cells. In addition to evaluation of cells made from this wide range of starting ingot properties, the minority carrier diffusion length was measured after various stages of cell processing to check if the processing had degraded the diffusion length of the original ingot.

1.2 Dependence of Silicon Solar Cell Characteristics on Silicon Properties

The solar cell is a large area, shallow PN junction, (PN diode) formed by thermally diffusing one conductivity type of impurity into silicon doped with the other conductivity type impurity. For this study, the N-type diffused layer was formed by diffusing phosphorous into P-type, boron doped wafers.

In the power generating (photovoltaic) mode of operation, the junction collects current carriers generated by absorption of sunlight at various depths of penetration

of sunlight into the silicon. These carriers can move from their point of generation, and if their lifetime is sufficient, they move to the PN junction region and are collected as useful current. The PN junction has a built-in voltage between the P and N regions; the power generated by a solar cell is derived from the passage of the collected charge carriers through this junction voltage.

Several properties of a silicon crystal can control cell characteristics.

(a) Influence of Resistivity

The resistivity of the starting silicon (P-silicon in this case) is determined by the boron doping concentration and is given by the expression

$$\rho = \frac{1}{qN_A\mu} \qquad (1)$$

where q is the electronic charge,

N_A is the acceptor (boron) concentration, and

μ is the mobility of holes.

The light-generated properties of the solar cell are related to the silicon diode characteristics by the following equation:

$$I_L = I_{sc} - I_o \left(\exp \frac{qV_L}{AkT} - 1\right) \qquad (2)$$

In this equation, the voltage V_L and the current I_L represent the electrical output of an illuminated solar cell operating into a fixed external load, and I_{sc} is the current obtained when the cell load terminals are short-circuited. The second term on the right hand side of (2) describes the PN junction

characteristics. Here q, k, and T have their usual meaning (electronic charge, Boltzmann's constant, and absolute temperature), and A is a correction factor indicating deviation from an "ideal" diode (where A = 1). The diode saturation current, I_o, expresses the silicon properties which control the PN junction characteristics. For a simple case (diffusion diode theory[22]), I_o is given by:

$$I_o = q \frac{n_i^2 D_p}{N_D L_p} \coth \frac{W_n}{L_p} + q \frac{n_i^2 D_n}{N_A L_n} \coth \frac{W_p}{L_n} \qquad (3)$$

where $N_{D,A}$ is the dopant concentration influencing resistivity,

$L_{p,n}$ is the minority carrier diffusion length,

and n_i, D, W refer to the intrinsic carrier concentration, the diffusion coefficient of the carriers, and the thickness of the silicon.

For most solar cell structures, the base region component of I_o (the second term in (3) in this case) is usually very much larger than that contributed by the diffused layer (the first term in (3)), and thus the diode characteristics depend primarily on the silicon material properties of the P-type base; i.e.,

$$I_o \approx q \frac{n_i^2 D_n}{N_A L_n} \coth \frac{W_p}{L_n} \qquad (3a)$$

Similarly the maximum voltage obtainable from the solar cell at a given illumination level (corresponding to the case where the cell load terminals are left open circuited) is given by:

$$V_{oc} \approx \frac{AkT}{q} \ln \frac{I}{I_o} sc- \qquad (4)$$

High resistivities (N_A low) generally have high L_n-values. Since I_{sc} increases for higher L-values, high resistivity silicon can lead to higher I_{sc} values (and conversely, low resistivity leads to lower I_{sc}).

The obtainable range of N_A values (from 10^{13} to 10^{20} cm^{-3}) is much larger than the corresponding range of L_n values ($\approx$300 to 5 μm), meaning that N_A has the strongest influence on determining the I_o-value in equation (3a).

Since high N_A means lower I_o, lower resistivities would be expected to lead to higher voltages V_{oc}, by (4).

The above considerations explain the statement made in the introduction above. This program examined the silicon properties and the behavior of cells over a fairly wide range of N_A and L_n values, to see if the above theoretical expressions were reliable in predicting cell behavior.

(b) Considerations on Minority Carrier Diffusion Length

(i) Unwanted Impurities

In addition to dependence on the background doping, L can be determined by the other properties of the silicon.

In particular, the presence of very small concentrations ($\approx 10^{12}$-10^{14} cm^{-3}) of any of several harmful impurities (including gold, iron, and copper) can cause serious decrease in L, because these impurities can seriously increase the carrier recombination.

Thus some of the precautions described below are empirically selected (by continued useage in normal cell processing) to reduce the chance of accidental introduction of sufficient concentration of these "killer" impurities.

(ii) Other Impurities

Although not as serious in their effect as the impurities discussed in (i), there is the chance of introduction of impurities other than boron into the silicon crystal. These impurities may be a byproduct of the purification process for the silicon used for the growth of the silicon crystals (e.g. carbon), or may be the result of the growth conditions (e.g. introduction of oxygen from the quartz crucibles used to hold the molten silicon during crystal growth).

(iii) Crystallographic Perfection

The diffusion length for carriers is reduced if they cannot move freely through the crystal lattice. Although all the crystals used here are single crystal, (meaning that no grain boundaries are included), there is still the chance of internal crystal imperfections such as dislocations or clusters of impurities.

It can now be appreciated better why the ingots specified for this program included a wide range of intentional boron doping concentrations, high and low values of oxygen concentrations (oxygen could possibly interact with other impurities or crystal defects, thereby affecting L-values), and a range of dislocation density values.

1.3 Current Experimental Situation

The extent of the information on the dependence of solar cell properties on the silicon resistivity is summarized by Figures 1 through 4.

Figure 1 shows the dependence of L on resistivity for N-silicon; the decrease in L for decreased resistivity is seen.

Figure 2 gives the dependence of J_{sc} for a cell on L;[4] the measurements were made under simulated space sunlight (called air mass zero, AM0).

All cells were ≈12 mils thick and were made from 10 ohm-cm P-silicon, and the diffusion length was systematically decreased from the starting values ($\gtrsim 150\ \mu m$) by exposure to increasing dosages of 1 MeV electrons. J_{sc} is seen to decrease rapidly for $L \lesssim 100\ \mu m$; the slow rate of change for the higher L-values can be explained by the fall-off in the fraction of the solar spectrum which penetrates to depths greater than $150\ \mu m$; thus even if the carriers have greater diffusion lengths, there are relatively fewer carriers generated to contribute to I_{sc} by moving to the PN junction. Using a combination of curves like Figures 1 and 2, the dependence of J_{sc} on resistivity can be estimated. Figure 3 shows such a curve, with some measured values indicated by squares.

Figure 4 shows the theoretical* and observed variation of the maximum voltage obtained from cells (under AM0 illumination), as the resistivity of the bulk silicon was varied. This figure shows again the interest in determining the causes for V_{oc} fall-off for resistivities

* using the simple theory outlined in Section 1.2

below 0.5 ohm-cm, because attaining V_{oc} values closer to the theoretical values would result in significant increase in cell output.

2.0 EXPERIMENTAL DETAILS

2.1 Description of Special Ingots

Table 1 lists the properties and specifications of the ingots used for this study. The ingots were boron-doped to be near 0.01, 0.05, 0.1, 1, and 10 ohm-cm. The ingots had either high or low concentrations of oxygen or dislocations.

The oxygen content was a result of the method of ingot growth; ingots with high oxygen concentration were crucible-grown, those with low oxygen content were grown without a crucible.

The dislocation density in the silicon ingots was influenced by the perfection of the seed crystal, and by the crystal growth conditions--mainly the speed of growth and the temperature gradients present while the crystal was growing.

2.1.1 Sample Preparation

The ingots were all grown in the (111) direction, and all slices were cut perpendicular to the growth axis, thus ensuring that the slices were in the (111) plane. The slice cutting to 2 x 2 cm squares was carried out by an internal diameter diamond-edged saw blade, with water cooling to minimize crystal damage during cutting.

For each ingot, the following slices were cut:

(a) A thick slice ($\approx$0.100 in.) was cut near the end of each ingot and chemically polished by etching in a mixture of HF and HNO_3 ($\approx$1 HF: 4 HNO_3). For all ingots except # 10, 11, 12, Schottky metal-silicon collecting barriers* were applied to one

* See Appendix B2 for details of these barriers.

polished face; the opposite face was then sand-blasted, and an open-structure ohmic contact pattern was applied by evaporating titanium-silver metals through a metal shadow mask.

Figure 5 shows the structures used.

These samples were used to determine the diffusion length for the unprocessed ingot.

(b) The remaining ingot was sliced to give slices of thickness greater than twice the diffusion length as estimated from the manufacturer's measurements on the ingots (or from prior experience with silicon ingots).

These slices were all lapped to 5 μm finish and were then mechanically-chemically polished, using the Lustrox process.

The slices were divided into several groups.

(i) A few slices ($\approx$ 5) were treated as described in (a) above, to provide additional samples to evaluate diffusion length before any further processing.

2.1.2 Cell Processing Sequence

The remaining slices were taken through the cell processing sequence shown in Table 2. A drop-sequence was used, i.e. several slices were removed after the major process steps shown in Table 2.

(ii) Those slices which passed through the complete sequence of process steps were evaluated as solar cells.

(iii) The other slices were sandblasted on the back face, had an open metal contact structure applied to this side, and had a full contact applied to the diffused side (like Figure 5), for use in diffusion length measurements.

(iv) Some of the slices from steps I and II were chemically polish-etched and were then placed in Sirtl etch[17] to form etch pits at edge dislocations. For these slices the dislocation density was measured, to compare to the density quoted by the ingot supplier, and also to check whether the dislocation density had changed during diffusion.

(v) On some of the diffused slices, small areas were isolated by masking and were then etched to form a number of "mesa" PN diodes. The unilluminated forward diode characteristics were measured on these mesa diodes.

2.1.3 Precautions Taken in the Processing

The cell process sequence used was a proven manufacturing procedure. As far as possible, at all stages of sample and cell preparation, care was taken to minimize the introduction of impurities which could affect the silicon properties (see 1.2 (b) (i)).

This care extended to the use of high purity cleaning solutions (electronic grade solvents and acids) and deionized water. Also the metals and chemicals used were purified (contact metals 99.99% silver, 99% titanium, high purity $POCl_3$ as the diffusant source). The gases (nitrogen, oxygen, or forming gas) used during

diffusion, annealing, or sintering were dried and were of good commercial purity.

To minimize penetration of any impurities left on the silicon surface, the temperature-time schedules were reduced as much as possible. The right hand column in Table 2 indicates the typical processing temperatures involved at each process step.

The holding fixtures, used during the liquid rinsing, and the furnace tubes, were carefully cleaned and were used specifically for the separate operations.

Care was taken in handling (minimum pressure from holding fixtures or tweezers) to reduce the chance of mechanical damage to the shallow PN junction.

2.2 Measurement Methods Used

The main measurement methods are described.

2.2.1 Resistivity Measurements

Four-probe methods (with suitable correction factors) were used to measure the resistivity of the starting ingots and slices and for sheet resistance measurements on the diffused layers. In addition, measurement of the zero bias capacitance provided a cross-check on the dopant concentration at various stages of cell processing.

2.2.2 Etch Pit Density Measurements

The Sirtl etch (2.1.2 (iv) above) attacked edge dislocations preferentially, leaving tetrahedral pits on the (111) plane. The density of these etch pits was estimated by photographing known areas at typical locations

across the slice and by counting the number of etch pits in that area. The results obtained using the Sirtl etch are given in Table 3. With a few exceptions, the counts are seen to agree with the specifications given for the ingots. Other etchants (e.g., Dash etch*) were used and gave similar densities to the Sirtl etch.

2.2.3 Solar Cell Measurements

On samples which had been processed to form solar cells, measurement of the I-V characteristics was made by varying the load resistance from zero to a high value, while the cell was illuminated. From the I-V curve, I_{sc}, V_{oc}, and the maximum power, P_{max}, could be read-off; also the CFF which equals $P_{max}/I_{sc} \times V_{oc}$. In addition, an indication of the spectral response was possible by measurement of I_{sc} under either the xenon or tungsten lamps which were blended in the simulator to provide the AM0 spectrum. Thus, the xenon I_{sc} showed the response for short wavelengths ($< 0.6\ \mu m$), whereas the I_{sc} under tungsten gave the response for longer wavelengths ($> 0.6\ \mu m$). Detailed spectral response curves were measured using a filter wheel monochromator.

2.2.4 Diffusion Length Measurement

The carrier diffusion lengths (or lifetimes) were measured over the wide range of resistivities (0.01 to 10 ohm-cm) and the consequent expected wide range of diffusion lengths (< 10 to $> 200\ \mu m$). The factors considered in choosing the measurement method are given in Appendix A. Appendix B describes the chosen method (the photovoltaic method), both from theoretical and practical aspects. Two methods were used:

* Dash etch: 1 HF, 3 HNO_3, 8 CH_3COOH for 16 hours.

(a) Back Current Method

Here a collecting barrier (diffused PN junction or Schottky barrier) was formed on one side of the slice together with an ohmic contact; the other side of the slice was sandblasted to ensure high surface recombination velocity at that surface, and an open structure ohmic contact was applied, allowing the test illumination (LED, etc.) to fall directly on the sandblasted silicon. This structure is shown in Figure 5.

(b) Front Current Method

In this method, the test illumination fell directly on the collecting barrier (through an open structure contact) the other side of the slice had an ohmic contact applied over the slice.

2.2.5 Diode Measurements

For no illumination, the diode I-V characteristics could be measured on samples which contained a PN junction. The I-V characteristics were measured for either forward or reverse bias polarity. Also the same dark diode characteristics could be measured, as a function of position over the whole cell area, by diode measurements made on small mesas, formed as in 2.1.3 (v).

2.2.6 Trap Density Measurements

The presence of harmful impurities can lead to traps which reduce carrier diffusion length.

Three methods were tried, to find trap densities.

(a) Variation of Diffusion Length with Temperature

Careful measurement of L as a function of temperature (either increasing or decreasing from room

temperature), with simplifying assumptions about the trap properties, could lead to information concerning trap densities, and their level in the forbidden energy band of silicon.

(b) Thermally Stimulated Currents

References (19-21) describe this measurement method. A sample with some mesa diodes was cooled to liquid nitrogen temperatures. The diodes were illuminated with penetrating radiation, thus exciting excess carriers into traps. With a constant reverse voltage applied to the diodes, the sample was warmed up to room temperature. Whenever the temperature provided enough thermal energy to empty a trap level, a burst of excess dark reverse current was observed. The temperature at which the burst occurs could be used to show the trap energy level. The magnitude of the current pulse at this temperature showed the density of traps at that level.

(c) Thermally Stimulated Capacitance

Reference 21 describes this method which is similar in principle to method (b), but which offers some advantages.

Again a mesa diode was used. The capacitance at large reverse bias was measured for two initial starting conditions, either by cooling the diode (under zero bias) to low temperature (liquid nitrogen), then applying reverse bias and warming the diode, or by applying the reverse bias at room temperature before cooling, and again measuring the change in capacitance as the sample returned to room temperature.

3.0 EXPERIMENTAL RESULTS

3.1 Diffusion Length Results

3.1.1 Diffusion Length versus Processing Step

Figures 6 through 9 summarize the L-values measured on fifteen ingots* after the main process steps, the steps being shown on the bottom of the figures. An envelope curve is used to indicate the range of measured values. Generally, the spread in L-values is reasonably low, allowing the plotting of average L-values as given in Figure 10. On this figure, the ingot parameters have been included. It can be seen that the diffusion length did not suffer a marked change at any step as was originally expected before this program. There did not appear to be any correlation between the direction of L-change and the resistivity or the oxygen content. The low dislocation density ingots showed some tendency to decreased L after diffusion.

3.1.2 Diffusion Length versus Silicon Properties

Using L-values for samples completely processed as cells (i.e., after Step VI in Figure 10), L is plotted versus resistivity in Figure 11. On this figure, each ingot point is identified by two letters, the first letter indicating the extreme of oxygen concentration, the second letter showing the extreme of dislocation density. L fell off rapidly for resistivity below 0.05 ohm-cm (for $N_A > 10^{18}$ cm^{-3}). Also using published values[16] of carrier concentration versus resistivity, L is plotted as a function of the acceptor concentration, N_A, in Figure 12. Reference 16 also gives the measured variation of carrier mobility (μ) with carrier concentration.

* The two remaining ingots, 973-8 and 9 are discussed separately in section 3.3.1 below.

Since the diffusion coefficient for carriers is given by the Einstein relation

$$D = \frac{kT}{q} \cdot \mu \qquad (5)$$

and since

$$L^2 = D\tau = \frac{kT}{q} \mu\tau \qquad (6)$$

(where τ is the minority carrier lifetime), use of the μ-values corresponding to various N_A values results in a set of τ-values corresponding to the L-values measured. In this way a plot of τ versus N_A can be obtained from Figure 12 and is shown in Figure 13.

Also shown in Figure 13 is a plot of carrier lifetime versus the concentration of gold, a widely-used lifetime killer.

3.1.3 General Comments on L-measurements

L did not change appreciably with the various process steps. In general, L decreased as the background doping was increased. For any given carrier concentration, the L-values for low oxygen concentration ingots were higher. However, these low oxygen ingots were grown by some modification of float-zone refining, so that it could be that the higher diffusion length resulted from improved crystal growth conditions rather than from the low oxygen content.

The plot of τ versus the gold concentration, in Figure 13, was included to see if the rapid decreases in τ with dopant concentration for $N_A > 10^{18}$ cm^{-3} could be attributed to the accidental incorporation into the silicon of an impurity like gold (or iron), carried in with the boron dopant source. If the dopant source contained a

fixed percentage of such an impurity (say ~0.1%), then part of the τ-decrease at the increasing N_A values could be caused by the increasing concentration of the killer impurity.

The dislocation densities did not appear to have a strong effect on L, since for each resistivity range comparable L-values were obtained with either high or low dislocation densities. There has been speculation* that since almost all the ingots with high dislocation density showed increased L after diffusion, there was the possibility of dislocation-gettering, i.e., the dislocations aided in off-setting some of the impurities responsible for decreasing L.

3.2 Solar Cell Results

Solar cell measurements were made for samples processed through step VI. From the I-V curve traced under AM0 illumination, intensity 140 mW/cm^2, (and the cells at 28°C), the main photovoltaic parameters, short circuit current (I_{sc}) and open circuit voltage (V_{oc}) were extracted and plotted.

3.2.1 Cell Current Values

Figure 14 shows how I_{sc} varied with N_A. Figure 15 shows the plot of I_{sc} versus diffusion length, L. (For comparison, Figure 2 is replotted as a dashed curve on the same scale.) The ingot numbers and their resistivity are given alongside the experimental points. In many cases, after cell measurements had been made, the back contact was partially removed, and the L-value for the cells was measured directly by the back current version of the photovoltaic method for measuring L.

* Private communication from H. W. Brandhorst, Jr., NASA-Lewis Research Center.

As L decreases, I_{sc} is also seen to decrease. The experimental slope differs from that of Figure 2, because that figure was obtained by reducing L (by electron irradiation) while maintaining the original resistivity (10 ohm-cm). For the ingots in the present study, L was decreased by the additional acceptor doping, and the material quantities connecting the diffusion length and I_{sc} (mobilities, diffusion coefficients) will be different for different doping levels.

Spectral response curves are plotted in Figures 16 and 17 along with typical L-values. The losses in I_{sc} at higher doping levels (lower L) show reduced collection (by diffusion) of carriers generated deeper in the silicon by more penetrating wavelengths.

3.2.2 Cell Voltage Values

Figure 18 shows V_{oc} as a function of carrier concentration. The highest V_{oc} values occurred around $N_A = 7 \times 10^{17}$ cm^{-3} (resistivity $\approx$ 0.1 ohm-cm) and fell off predictably at lower concentrations, and for concentrations above 10^{17} cm^{-3} were less than the simple theoretical V_{oc} values plotted in Figure 4.

The experimental curves in Figure 4 and Figure 18 do not agree exactly; the reason is that Figure 4 was based largely on measurements on P+/N cells, and since $\mu_n > \mu_p$, to give equivalent resistivities requires concentrations of donors smaller than the acceptor concentration. The data given in Figure 18 represents more systematic information for P-ingots, over a wider doping range, than was available earlier.

Below (in section 4.0) some speculation is given on the possible causes for the reduced V_{oc} values at high doping concentrations.

3.3 Other Results

3.3.1 Measurements on Ingots with High L-values

For two of the ingots (973-8, 973-9) with resistivities approximately 10 ohm-cm, the vendor measured very high minority carrier lifetimes (400 μs, 800 μs respectively, corresponding to L $\approx$ 1150 and 1625 μm).

These ingots were treated somewhat differently from the other ingots, because it was hoped that they would give very high I_{sc} values, and would also allow checking of the assumptions made in the photovoltaic method selected to measure L-values.

Unfortunately, this was not the case. The solar cell measurements on slices cut from these special ingots did not show any improvement in I_{sc} resulting from the high L-values; in fact, the spectral response curves for cell from these ingots showed reduced long wavelength response.

The L-values measured on both undiffused and diffused specimens of these ingots were high, in the range of those quoted by the vendor (who used a photoconductive decay method for τ-measurement). However, the various methods used to analyze the photovoltaic L-method were not internally consistent. More details of the measurements on these ingots is given in Appendix B.

3.3.2 Unilluminated Diode Characteristics

Additional information to explain the differences in cell voltage measured for the various ingots was obtained

by taking typical cells using silicon of 10, 1, or 0.1 ohm-cm, and dividing the cells into several separate mesa diodes (by masking and etching). The forward biassed I-V characteristics with the diode illuminated were then plotted for each mesa diode.

In general it was found that at the higher resistivity (>1 ohm-cm) these small area diodes had very uniform behavior, but that the spread in characteristics became progressively wider as the resistivity decreased. Figure 19 shows the measured spread in forward voltage (V_f) needed to produce a forward current equal to 35 mA/cm^2 (the operating current density of the diode for an illuminated solar cell). Although the maximum V_f increases for the lower resistivities, the increasing fraction of the mesas with low V_f results in seriously decreased V_{oc} for the cell, because in the cell all those mesa diodes operate in parallel, and low voltage for any small area can decrease the available V_{oc}.

Figure 20 shows the envelope of the measured ln I_f versus V_f curves for three resistivities.

Some other tests were run wherein the PN junction depth was increased to approximately one hundred times that used in solar cell PN junctions; in most cases the same trend in V_f was observed at the lower resistivities.

Figures 21 and 22 show the envelopes for two resistivities for various junction depths.

The implications of these measurements are discussed more fully in section 4.0.

3.3.3 Trap Density Tests

Three different methods (see 2.2.6) were tried, to give an indication of the trap density, or of the approximate position of the trap level in the forbidden energy gap.

None of these methods was satisfactory, for the following reasons.

(a) Variation of L with Temperature

L-measurements were made using the I_b method over a a range of temperatures of the samples. However, serious experimental difficulties were met. First at lower temperatures, the back illuminated sample was covered with a layer of frost, and effective, repeatable optical transmission from the light source into the sample was difficult. Second, the absorption coefficient of the sources was strongly temperature dependent, leading to uncertainties in the "constants" to be used in the equations. Attempts were made to cancel out these experimental factors by measuring L using the ratio of the currents on each side of a step in the sample. However, as mentioned in Appendix B, the L-value obtained from the step samples did not agree with that measured on the separate sides of the step, thus this method did not give reliable results.

(b) Thermally Stimulated Currents

Mesa diodes were formed. However, on cooling down they already had large (and unstable) reverse leakage currents. Later tests used specially made planar passivated diodes formed in typical ingots, but no

current bursts were seen on following the procedure listed above in 2.2.6 (b).

(c) Thermally Stimulated Capacitance

Experimentally, this method appeared promising, but in practice there was hysteresis which prevented obtaining repeatable capacitance values. Also the trap densities were probably very low for high resistivity silicon (long diffusion length). For the lower resistivity ingots where the trap density could be expected to be higher, the large impurity content led to high background capacitance, thereby resulting in the need to measure small percentage changes in capacitance. The tests run did not lead to more than an order of magnitude indication (10^{14} traps per cm^3 for 1 or 10 ohm-cm silicon).

3.3.4 Gettering Tests

Because it was realized that the lifetime was determined by ingot growth conditions, experimental attempts were made to reduce the number of effective traps by subjecting typical slices to various "gettering" treatments. In these treatments, a liquid phase was maintained at the silicon surface for a period long enough for fast-diffusing impurities such as iron, gold, or copper to reach the surface from the bulk of the slice. The liquid phase can act as a sink for these killer-impurities, and on cooling the sample, and removing the surface layers, it is possible to obtain a slice with reduced trap centers. Experimentally, gettering tests were run on both 0.01 and 0.1 ohm-cm ingots, using either aluminum or phosphoro-

silicate glass as the liquid phase. The results were negative in that the measured diffusion lengths after gettering were the same as the L-values measured before gettering.

4.0 DISCUSSION OF RESULTS

This study began with the assumption that the quality of silicon ingots (as shown by minority carrier lifetime in particular) was altered as a result of solar cell processing. The results showed that this was not the case, for the processing methods and materials used here. There were relatively small changes in the measured values of diffusion length and dislocation density. The results can be summarized as follows:

4.1 Diffusion Length Measurements

The photovoltaic methods analyzed and tested in this work proved effective over the wide resistivity range (0.01 to 10 ohm-cm) and over the large range of diffusion length values (2 to 1600 μm). (The corresponding lifetime range is even larger, from 10^{-2} to 700 μs.) For starting ingots, measurements could be made for resistivities $\geq$ 0.05 ohm-cm. The L-values obtained could be related directly to the current collection properties of solar cells. The measurements were repeatable, and the accuracy was better than that obtained in most other lifetime or diffusion length measurements. No drastic change in the basic methods was needed over the whole range of measurements.

4.2 Diffusion Length Values

Figures 6 through 9 show that L for a given ingot did not vary largely for the cell processing used here. This implies that the processing methods did not add a significant number of harmful impurities. On the other hand, large L-variations were obtained from ingot to ingot. The variation of L with other parameters

(Figures 11 and 12) showed that L decreased drastically for acceptor concentrations above 5×10^{17} cm^{-3}, and that in general ingots grown without use of a crucible had higher L-values.

The cause for decreased L at low resistivities depends on starting ingot properties and appears to be related to the intentional boron doping. The decrease in L up to 10^{18} cm^{-3} resembles the decreased hole mobility to this concentration. However, the large decrease in L for concentrations above 10^{18} cm^{-3} is greater than that expected from the mobility decrease caused by impurity scattering.

The curves given in Figure 13 suggested that killer-impurities like gold are possibly being added with the boron. The negative gettering tests described in section 3.3.4 suggest that if such impurities are the prime cause for L-decrease, their distribution was not altered much by the gettering treatments used.

The L-values correlated well with the cell I_{sc} values, and also with the cell spectral response.

4.3 Low Resistivity Silicon Results

The present work added more information on the variation of solar cell properties over a wider range of resistivities.

(a) Several well-controlled ingots at both 0.1 and 0.01 ohm-cm were evaluated. These ingots had a wide variety of concentrations of oxygen and dislocation density.

(b) The diffusion length of these low resistivity ingots was measured, and the values obtained could explain the I_{sc} fall-off observed in cells made from these ingots.

(c) Some reasons for the cell V_{oc} behavior (did not increase, as earlier theories predicted, with fall-off increasing at lower resistivities) were found in detailed study of the large area PN junctions via measurements of the dark diode behavior of small mesas.

4.3.1 Speculation on V_{oc} Results in Low Resistivity Silicon

In section 3.3.2, it was observed that as the bulk resistivity was decreased, there was an increased fraction of mesas with low V_f, even though the maximum V_f values were higher at lower resistivities. Thus a possible physical mechanism for decreased V_{oc} for cells was the increasing chance of small areas of the junction contributing excess forward current.

Figure 23 (curve with squares) shows the best V_{oc} values obtained versus the acceptor concentration. Also shown are two curves showing V_{oc} values obtained by considering two different theoretical models. Table 4 lists the measured values used in these theoretical estimates and gives the derived values which were used to plot the curves.

The two theoretical cases are:

(a) Diode Diffusion Theory[22]

Saturation current density (J_{OD}) is given by:

$$J_{OD} = \frac{q n_i^2}{N_A} \sqrt{\frac{D_n}{\tau_n}} \qquad (7)$$

where n_i is intrinsic carrier density,

N_A is acceptor concentration,

D_n is diffusion coefficient for electrons, and

τ_n is lifetime for electrons in bulk silicon.

The best measured values of τ_n are shown in Table 4, and these values are combined with the D_n and N_A values shown to derive J_{OD}.

In turn $(V_{oc})_D$ is derived from:

$$(V_{oc})_D = V_T \ln \frac{J_{sc}}{J_{OD}} \qquad (8)$$

where $V_T = \frac{kT}{q}$ and

J_{sc} = short circuit density taken as 35 mA/cm^2.

These V_{oc} values are shown by circles in Figure 23.

(b) Space-Charge Recombination Theory

Saturation current density is given by:

$$J_{os} = \frac{qn_i W}{2\tau_e} \qquad (9)$$

where n_i = intrinsic carrier density,

W = space charge layer width, and

τ_e = effective carrier lifetime in the space charge layer.

Reference to published results showed that a reasonable value for τ_e was $\approx \frac{1}{150}\tau_n$. Using this estimate, together with measured values of W (obtained from capacitance measurements), gave the values of J_{os} in Table 4.

Again,

$$(V_{oc})_s = 2V_T \ln \frac{J_{sc}}{J_{os}} \qquad (10)$$

These values are shown by crosses in Figure 23.

In general, V_{oc} appears to be following the diffusion diode theory for low acceptor concentrations. The deviations from this classical theory are more pronounced for $N_A \geq 10^{16}$ cm^{-3}. Analytically the experimental trend suggests an increasing effect of the space charge recombination centers for $N_A \geq 10^{17}$ cm^{-3}, until finally for $N_A > 10^{18}$ cm^{-3}, the V_{oc} values are dominated by the recombination centers. It is not obvious why the V_{oc} values can be approximated by choosing τ in the space charge layer much less than the τ value measured in the bulk. The J_o values derived here agree reasonably well with extrapolations at high (J_{OD}) or low (J_{os}) current densities for the ln I_f versus V_f plot.

As discussed in section 5.0 below, much work remains to complete the explanation of the V_{oc} values obtained.

4.3.2 Other Possible Mechanisms

The speculation in the previous section assumed two limiting cases, namely the diode diffusion theory, and space charge recombination theory. However, the precise responsible mechanism has not been identified.

Other work funded by NASA-Lewis Research Center[24] has led to the conclusion that PN junctions formed in low resistivity silicon have excess leakage caused by channelling effects.

Calculations show that usually much higher doping levels than those considered here are necessary for the onset of junction tunnelling. However, the measured depletion layers were thin (down to 500 Å), and with the increased density of recombination centers in the space charge layer, tunnelling may be possible.

It is possible that the failure of Schottky barriers found at resistivities below 0.05 ohm-cm is also caused by a similar mechanism to that which decreases V_{oc}.

4.4 Relevance of Program to Objectives

The objective was to study the effects of processing on silicon properties, especially on carrier lifetime. The program revealed that conventional solar cell fabrication technology does not have as marked an effect as previously thought on the silicon properties. These properties are fixed more by the conditions occurring during ingot growth.

For the ingots with high doping concentrations, a fall-off in diffusion length was measured, with corresponding decrease in cell current. This current decrease was accompanied by a decrease in open circuit voltage at the highest doping levels used ($> 10^{18}$ cm^{-3}).

Thus the original program objective was met; however, the experimental work revealed new areas of work required to elucidate the behavior of cells made from highly doped silicon.

4.5 Implications for Future Improvements in Cell Output

In order to increase cell output further by use of lower resistivity silicon, two physical processes must be understood, and if possible, offset.

(a) The cause of decrease in diffusion length must be identified.

(b) The causes of excess diode currents must be isolated, and if possible remedial processing applied to allow higher voltages.

5.0 CONCLUSIONS

The following conclusions can be drawn:

(a) Present-day solar cell processes did not have a marked effect on the properties of silicon, for ingots covering a wide resistivity range (0.01 to 10 ohm-cm), and including extreme values of oxygen content and dislocation density.

(b) The properties of solar cells made from those ingots indicated that the I_{sc} behavior could be correlated with the measured values of diffusion length, and that the V_{oc} behavior could not be easily explained.

(c) The physical cause for reduced L at high doping levels was not clearly identified. Possibly the cause is a combination of effects caused directly by the higher concentrations of intentional dopant (boron in this case), and is also determined by increasing concentrations of "killer" impurities, accidentally incorportated in the growing crystal.

(d) The physical cause for slower increase of V_{oc} could lie in detailed examination of the causes of excess diode currents, with possible contributions from the same higher concentrations of intentional and unintentional impurities mentioned in (c).

(e) For all but the two ingots of very long diffusion length, the photovoltaic method of L-measurement described in the appendices proved more effective than many other methods used previously.

6.0 RECOMMENDATIONS

The following recommendations are made:

(a) To concentrate on ingots with doping concentrations greater than 10^{17} cm^{-3}, to identify the causes of reduced diffusion length, and increased diode current.

(b) To extend the trap density measurements to see if they can be used to aid understanding of the reasons for low L and higher I_o-values.

(c) To test ingots made with very highly purified dopant sources, e.g., use multiple zone-refining of the dopant ingot before it is used to grow the single crystal. This should be possible for the present case, since boron does not redistribute strongly on zone refining, whereas possibly the candidate metal impurities (like iron, gold, copper, etc.) will segregate and can be removed. Possibly also, some tests of gettering of the dopant source before its use in crystal growth could achieve the same objective.

(d) To continue work on measuring diffusion length, to ensure good correlation of this parameter with measured cell values. At present the photovoltaic method has good promise, as does the surface photovoltage method (see Appendix B).

7.0 REFERENCES

1. M. Wolf, Proceedings of 8th Photovoltaic Spec. Conf., (1970), p. 360
2. P. Iles, Proceedings of 8th Photovoltaic Spec. Conf., (1970), p. 345
3. H. W. Brandhorst, Proceedings of 9th Photovoltaic Spec. Conf., (1972), p. 37
4. R. W. Rostron, I.E.E.E. Trans., ED-19, (1972), p. 1024
5. ASTM Test F28-66, (1966)
6. Standards Committee, Proc. I. R. E.,49, (1961), p. 1293
7. A. P. Ramsa, H. Jacobs, F. A. Brand, Journ. Appl. Phys., 30, (1959), p. 1054
8. I. R. Weingarten, M. Rothberg, J. Electrochem. Soc., 108, (1961), p. 167
9. M. Waldner, J. Electrochem. Soc., (1959), p. 1005
10. M. E. Beatty, G. F. Hill, NASA TN D-2817, (1965)
11. W. Rosenzweig, Bell Syst. Tech. J., 41, (1962), p. 1573
12. E. O. Johnson, Journ. Appl. Phys., 28, (1957), p. 1349
13. A. M. Goodman, Journ. Appl. Phys., 32, (1961), p. 2550

14. C. Y. Chang, Y. K. Fang, S. M. Sze, Solid State Electronics, 14, (1971), p. 541

15. A. Y. C. Yu, Solid State Electronics, 13, (1970), p. 239

16. J. C. Irvin, Bell Syst. Tech. J., 41, (1962), p. 387

17. E. Sirtl, A. Adler, Z. Metallk, 52, (1961), p. 529

18. L. R. Weisberg, H. Schade, Journ. Appl. Phys, 39, (1968), p. 5149

19. H. Schade, D. Herrick, Solid State Electronics, 12, (1969), p. 857

20. L. Forbes, C. T. Sah, Solid State Electronics, 14, (1971), p. 182

21. C. T. Sah, W. W. Chan, H. S. Fu, J. W. Walker, Appl. Phys. Letts., (1972), p. 193

22. W. Shockley, Bell Syst. Tech. J., 28, (1949), p. 435

23. C. T. Sah, R. N. Noyce, W. Shockley, Proc. I. R. E., 45, (1957), p. 1228

24. E. Y. Wang, R. N. Legge, N. Christidis, "Excess Junction Current of Silicon Solar Cells," NASA grant NGR 23-006-057

APPENDIX A

DISCUSSION OF METHODS CONSIDERED FOR MEASURING DIFFUSION LENGTH

The measurement of diffusion length (L) was important in this study. Several factors were considered in choosing the method for measuring diffusion lengths.

(a) If possible, the method should be electrodeless to minimize alteration of the diffusion length by introduction of metallic impurities during the metal electrode formation. If this was not the case, the application of suitable contacts had to be performed at low temperatures to avoid the possibility that the sample preparation would affect the diffusion length. Previous work showed that 600°C was the threshhold for thermal stresses, and that temperatures below 400°C would be preferable to minimize introduction of harmful impurities like iron, gold, etc.

(b) The method should be applicable to both undiffused (starting silicon) and diffused samples.

(c) The method chosen had to be applicable over the whole resistivity range used here (0.01 to 10 ohm-cm) and over the expected diffusion length range (< 10 to > 250 μm). It was desirable that a single method be used over the whole range to avoid the need to correlate methods which measured slightly different parameters.

(d) The method used should provide L-values suited for correlation with solar cell I-V measurements.

A.1 Possible Diffusion Length Measurement Methods

To measure diffusion length (or lifetime) of minority carriers, two broad classes of methods are available. These classes can be described as transient or steady state methods.

A.1.1 Transient Methods[5-8]

In these methods the conductivity of the sample is modulated (e.g., by injection from a short pulse of light[5,6] or from a pulsed microwave oscillator[7,8]), and the rate of decay of the increased conductivity can be related to the carrier lifetime. In tests made early in this study, several difficulties were found for transient methods in meeting the factors given above. These difficulties were first, that when the carrier lifetime was short, the recovery pulse was very short and difficult to measure accurately; second, when the silicon resistivity was low (<1 ohm-cm generally) it was difficult to raise the energy of the input pulse sufficiently to produce a significant increase in sample conductivity without at the same time altering the assumptions inherent in these transient methods. In addition, at these high light or microwave intensities some of the boundary conditions became critical and the analytical solutions were complicated.

It was felt that the problems of the transient methods could be overcome by the steady state methods which will now be discussed in more detail.

A.1.2 Steady-State Methods[9-13]

In these methods, excess carriers are injected continuously (using light, microwaves, electrons, or current-injecting barriers) and the steady state conditions are used to

indicate the diffusion length of the injected carriers. For these steady state methods, fast transients do not have to be measured, and in addition, it is easier to measure steady currents more accurately over a very wide range, thus allowing measurement of a wide range of L-values. Three steady state methods were used in this work, the first two being described in less detail than the third, which was selected for this study.

(a) Surface Photovoltage Method[12,13]

For this method, a transparent, conducting contact is capacitatively coupled to the silicon and the photovoltages induced by light sources of different wavelengths are measured. If the equivalent light flux densities to produce the same surface photovoltage are plotted versus the reciprocal of the absorption coefficients for the illuminating wavelengths, the intercept of the line obtained on the zero flux density axis gives the diffusion length. Some workers have reported good success with this method even down to 0.1 ohm-cm. An ohmic contact is required for the back surface of the samples, but a low temperature contact (pressed indium) has sufficed. Initial tests in this work did not give repeatable results. However, this method has been successfully used both at the National Bureau of Standards, and also at NASA-Lewis Research Center.

(b) Transistor Gain Method

Whenever a diffused layer exists on the sample, it is possible to form a transistor structure by masking the diffused layer on both faces of a silicon slice and etching to

form an emitter-base-collector transistor structure. The current gain for such a wide base transistor can be measured and allows extraction of the diffusion length in the base. This method was not sensitive where the diffusion lengths were much smaller than the base width which was generally the case for lower resistivity material. Also for low resistivities there were large parasitic circulating currents in the transistor base, and these currents reduced the sensitivity of this method.

(c) Photovoltaic Methods[9,10]

For these methods carriers are provided by a light source and the resulting current and voltage at a collecting barrier are determined by the diffusion length, if suitable allowance is made for the boundary conditions. Sample structures as shown in Figure 5 can be used. Three main components of a sample can be seen--namely, the collecting barrier (a potential barrier which can collect minority carriers), a contact to this collecting barrier, and an ohmic contact to the silicon sample.

Two modes of illumination can be used as shown in Figure 5(a) and 5(b). For 5(a) (the back current, I_b method) the sample is illuminated on the surface opposite to the collecting barrier, and the injected carriers must move through the slice to reach the barrier and generate the measured photo current. In order to obtain measurable currents generated in material with very short diffusion lengths, very thin slices must be used. In 5(b) (the front current, I_f method) the sample is illuminated on the side with the collecting barrier. The carriers generated are collected at the barrier. This mode is more suited to silicon with

short diffusion lengths, since carriers are generated nearer the collecting barrier. For both modes the contact structure must have open areas on the face which is illuminated; typical examples are shown in Figure 5(c).

The use of these methods to measure diffusion length results in structures and measurements which closely resemble those used in actual solar cells. Therefore, correlation with the measured cell properties is direct. The theoretical and practical details of the photovoltaic methods are given in Appendix B (below).

(d) Electronvoltaic Method[11]

Another method to inject carriers uses moderate energy (~1 meV) electrons at low injection levels. This method requires separate measurement of some parameters (the number of hole electron pairs generated per incident electron) by subsidiary measurements, and has been regarded in previous solar cell work as a standard method. However, for the present work, a rapid, easily available method was needed. As will be seen in the next section, electronvoltaic measurements were made* on selected samples, which were then used to calibrate the photovoltaic method.

* At TRW Systems.

APPENDIX B

DETAILED DISCUSSION OF PHOTOVOLTAIC DIFFUSION LENGTH MEASUREMENTS

B.1 Theoretical Basis

The theoretical basis for the photovoltaic method for determining diffusion lengths is summarized here, giving the assumptions and practical equations used. The geometric arrangement is shown in Figure 24.

B.1.1 List of Symbols Used

α = absorption coefficient for photon-source

D = diffusion coefficient for minority carriers

τ = lifetime of minority carriers

L = diffusion length of minority carriers

ϕ_o = incident photon flux

n = density of carriers

S = surface recombination velocity

g = generation rate of carriers

q = electronic charge

A = sample area

W = sample thickness

B.1.2 General Assumptions Made in Deriving Equations

(a) Monochromatic illumination was used, characterized by a flux ϕ_o and an absorption coefficient α.

(b) One dimensional geometry used, i.e., the sample has large lateral dimensions compared to its thickness, and the intensity is uniform over the area illuminated.

(c) Unity collection efficiency obtained at the collecting barriers (PN junction or metal-semiconductor contact), i.e., any minority carrier reaching x = W, will be collected and contribute to current.

(d) A shallow PN junction depth such that x_J = junction depth $\ll \frac{1}{\alpha}$ (i.e., negligible number of carriers photogenerated in diffused layer for I_f method.

(e) Steady-state conditions (i.e., all variables independent of time).

(f) Homogeneous sample with no internal electric field. Therefore, α, D, and τ will be independent of x, and E (electric field) = 0.

(g) Low-level injection conditions such that α, D, and τ are independent of n, and E = 0.

(h) Back surface (x = 0) is a perfect sink for minority carriers (i.e., the back surface has a perfectly collecting metal-semiconductor barrier or the surface preparation is such that S_B is infinite).

B.1.3 Basic Equations

The basic equation for the study of spatial and temporal variations of minority carriers in semiconductors is the continuity equation. The continuity equation using the above-mentioned assumptions is:

$$g = \frac{n}{\tau} - D\frac{d^2n}{dx^2}$$

This equation is solved subject to the boundary conditions that at x = 0, n = 0 (i.e., for the I_b-method, the illuminated surface is a perfect sink for minority carriers),

leading to a derivation of the spatial distribution of carriers. Once the spatial minority carrier variation is determined, the front and back currents (I_f, I_b) can be determined as follows.

B.1.4 Back Current (I_b)

The general solution for I_b is still too complex for practical use. Thus the experimental conditions are adjusted to allow a simplified equation to be used. The experimental conditions are such that:

$$s \to \infty$$

$$(\alpha L)^2 >> 1$$

Then,

$$I_b = \frac{I_o}{\alpha W} \frac{\left(\frac{W}{L}\right)}{\mathrm{Sinh}\left(\frac{W}{L}\right)} \qquad \text{(B1)}$$

Here I_o is the current generated by the total incident flux ($I_o = qA\phi_o$).

Equation (B1) is useful for a determination of L. Once the $\frac{I_o}{\alpha}$ factor has been determined, e.g. by measurements on independently calibrated samples of known diffusion length, the diffusion length can be determined from the argument of the $\frac{\mathrm{Sinh}\left(\frac{W}{L}\right)}{\left(\frac{W}{L}\right)}$ function.

An alternate procedure is to use two samples of the same ingot (same L assumed) of different thickness W_1, W_2. Then take the I_b-ratio, thus yielding

$$\frac{I_{b1}}{I_{b2}} = \frac{\mathrm{Sinh}\ \frac{(W2)}{L}}{\mathrm{Sinh}\ \frac{(W1)}{L}} \approx \exp \frac{(W_2 - W_1)}{L} \qquad \text{(B2)}$$

(where $\frac{W}{L} >> 1$).

The value of L can then be determined by an iterative procedure. For the I_b method to be practicable it is necessary that the sample thickness be comparable to or larger than the diffusion length; ideally W should be greater than two or three diffusion lengths. On the other hand if the diffusion length is small, the $\frac{W}{L}$ factor may be so large that the back current becomes too small to measure accurately.

B.1.5 Front Current (I_f)

For the front current, it is assumed that the back surface is still a perfect sink for minority carriers (i.e., $S_B = \infty$) and the front surface PN junction is a perfect collecting barrier. If $\exp\left(\frac{W}{L}\right)$ is chosen to be $\gg 1$, then it can be shown that

$$I_f = I_o \frac{\alpha L}{1 + \alpha L} \qquad \text{(B3)}$$

For this expression to be useful to determine the diffusion length it is desirable that the factor αL not be too large, for if $\alpha L \gg 1$, then $I_f \simeq I_o$ and I_f is no longer a sensitive function of L. Using a calibrated sample of known diffusion length, the diffusion length of the unknown sample can be determined by taking the ratio of the forward currents,

$$\frac{I_{f1}}{I_{f2}} = \frac{L_1}{L_2} \cdot \frac{1 + \alpha L_2}{1 + \alpha L_1} \qquad \text{(B4)}$$

and solving (B4) for the unknown diffusion length. This solution is considerably simplified if αL_1 and αL_2 are both $\ll 1$. Then

$$\frac{I_{f1}}{I_{f2}} = \frac{L_1}{L_2} \qquad \text{(B5)}$$

One possible problem in using penetrating (low α) illumination so as to satisfy this condition is that of reflection from the back surface and bottom contact giving rise to multiple passes through the sample.

B.2 Practical Details of the Photovoltaic Method

This section describes the experimental conditions used to apply the theoretical equations above to use the photovoltaic (PV) method to measure diffusion lengths.

B.2.1 Sample Preparation

Section 2.2 described the sample preparation scheme used for all ingots. The thick slice ($\sim$ 0.10 in.) allowed estimates of the diffusion length for the as-received ingot. The choice of slice thickness was made to conform to the experimental conditions described in section B.1.

The slice surface conditions were chosen, either to provide an effective collecting barrier on one surface or to fix the surface recombination velocity on the other surface in the range required by the chosen solutions to the theoretical equations.

In some cases, the PV method could be used on solar cells; for the I_b method, much of the back contact of the cell was removed, and the open silicon surface lapped or sandblasted to increase surface recombination velocity. For the I_f method, the cells could be illuminated at the cell front surface.

B.2.2 Collecting Barriers

As described above, the diffusion length measurements depend on the presence of a barrier which can collect

photo-injected minority carriers effectively. Whenever a slice had a PN junction formed by diffusion, this PN junction could be used as the collecting barrier. For undiffused slices, a series of tests showed that metal-silicon Schottky barriers could be used as collecting barriers over most of the resistivity range used in this work. These tests involved forming a diffused PN junction, etching off half of the diffused layer and then applying a Schottky barrier to the etched portion. Open structure contacts were applied to the face opposite the two barriers, and the I_b resulting from a small area light spot was compared for the diffused barrier and the metal-silicon barrier. First moving the spot across the face opposite the PN junction gave constant I_b values showing that the diffusion length was constant across the slice. The collection efficiency of the PN junction was assumed to be unity. Generally the Schottky barriers had collection efficiencies greater than 0.80, and usually were above 0.90 (i.e., the I_b value for the Schottky barrier area was $\approx$ 0.9 the I_b for the diffused layer area). The repeatibility of the Schottky barrier formation was shown by etching off the barrier, replacing it with a fresh barrier, and measuring I_b; the collected currents for the two barriers showed close agreement.

It was found that effective Schottky barriers could be formed on all 10, 1, or 0.1 ohm-cm samples. For the 0.01 ohm-cm samples, the Schottky barriers were severely shunted, and this prevented repeatable measurements. A literature search[14,15] revealed that theory predicted and experiments confirmed that Schottky barriers formed

on silicon with resistivity less than 0.05 ohm-cm, were shunted because of the apparent onset of carrier tunnelling. Other attempts (using moderate temperature lithium diffusion or liquid metal barriers) were also unable to produce effective collection barriers. For these reasons, PV L-measurements could not be made for the 0.01 ohm-cm samples before they were diffused.

B.2.3 Light Sources

The equations given above in section B.1 showed that various solutions were possible depending on the absorption coefficient, and this parameter in turn was set by the choice of the light source. Several different sources were used, as follows.

(a) Light Emitting Diodes (LED)

LED's had several experimental advantages. They emit over a narrow wavelength band, and this band can be adjusted somewhat by varying the impurity doping in the LED.

Gallium arsenide LED's were used, emitting around 0.9 μm. Higher intensities could be provided by using an array of LED's.

The LED's used were physically small (the enclosing can was $\sim$ 3/16" maximum), and the emitted light was reasonably well collimated. Thus, when the LED was positioned close to the silicon surface, small areas could be illuminated. The LED wavelengths ($\sim$ 0.9 μm) were absorbed in approximately 2 μm depth in the silicon. The minority carriers generated in this 2 μm thick sheet could be regarded as a thin layer of carriers available for movement towards the collecting barrier. Despite the fact

that most of these carriers would be collected at the illuminated surface, (because the surface recombination velocity was maintained high intentionally) the resulting I_b was still measurable except for samples with very short diffusion lengths.

A convenient check on the PV experimental conditions was afforded by using two LED's of slightly different wavelengths (λ = 0.91 μm and 0.94 μm) mounted on the same header with a single glass window of high refractive index. Comparison of I_b values on a sample when each LED was switched in separately, gave a rapid check if the correct combination of sample conditions (collecting barrier surface recombination, slice thickness, and diffusion length) was being used.

(b) Sources with Low Absorption

For samples with low diffusion length, the front illumination method was used. In this case a source emitting long wavelengths (with low absorption) was needed. Tungsten lamps (which are rich in longer wavelengths) were combined either with a silicon filter (> ¼" thick), which prevented all shorter wavelengths from reaching the samples, or with a narrow band pass interference filter with transmission centered around 1.06 μm (accompanied by a 10 mil silicon slice to ensure no short wavelength leakage). For most of the L-measurements used in section 3.0, the 0.91 μm LED was used for the I_b method and the tungsten lamp with the 1.06 μm filter for the I_f method.

B.2.4 Measurement Circuit

To measure the true I_{sc} values even if the sample had high shunt leakage, the circuit shown in Figure 25 was

developed. A current to voltage converter was used. The effective resistance across the sample was 0.01 ohm. There was a low voltage drop across the sample equal to the measured voltage divided by 10^5, the voltage gain of the operational amplifier.

B.2.5 Calibration Procedures

As described above, the boundary conditions on the samples made were adjusted to give equations (B1) and (B3) for the I_b and I_f respectively.

These equations were:

$$I_b = \frac{I_o}{\alpha W} \frac{\left(\frac{W}{L}\right)}{\text{Sinh}\left(\frac{W}{L}\right)} \qquad \text{(B1)}$$

$$I_f = I_o \frac{\alpha L}{(1 + \alpha L)} \qquad \text{(B3)}$$

Several different calibration procedures were used.

(a) Use of Samples Calibrated by Electronvoltaic Measurements

Several solar cells covering a range of diffusion lengths had their diffusion length measured* by the electronvoltaic method (EV method).

These calibrated cells were then processed to provide samples suited for photovoltaic measurements of diffusion length using either front or back illumination.

For each series of L-measurements these calibrated samples covering the expected L-range were used to check the $\frac{I_o}{\alpha}$ (or I_o) value for the particular light source, spacing, etc.

* Measurements made by J. R. Carter, Jr., of TRW Systems.

(i) I_b Method

Table 5 lists the EV measurements of diffusion length for five cells which had an open back contact to allow back current measurements. The cell thicknesses (W) and values of the function $\frac{\text{Sinh } (W/L)}{(W/L)}$ are given. Using equation (B1) I_o/α was computed, and the resulting values are also tabulated. If conditions were maintained constant, this value of I_o/α could be used for subsequent measurements using the back current. In practice, the LED-sample spacing and other conditions varied slightly for each series of measurements, but by cross-checking with these calibrated EV samples, the applicable I_o/α for each series was derived and used.

(ii) I_f Method

Table 6 lists EV measurements of diffusion length for five other cells with lower diffusion lengths. On these samples, measurements of front current were made, using a longer wavelength (lower absorption coefficient) source, namely, a tungsten lamp and a 1.06 μm filter. The I_f values are shown in Table 6, and are plotted versus L in Figure 26. As for the I_b-method, for each series of I_f measurements, some of these calibrated samples were used to derive the constant I_o in equation (B3) above.

The absorption coefficient values (α) in the above equations were measured experimentally, as shown in Table 7. However, the sources were not strictly monochromatic, so that some error was inherent in using "effective α-values". Where possible, constants such as I_o/α were derived from the calibrated samples and used in the measurements on the various ingots.

(b) Use of a Standardized Photocell

Using a solar cell whose absolute spectral response had been measured by the National Bureau of Standards, it was possible to estimate the effective photon output of the light source around its emitted wavelength. In turn the photon current entering the silicon sample could be calculated by applying applicable transmission coefficients. Figure 27 shows the absolute spectral response of a cell used to measure the photon output of two light sources. These sources were LED's with emitted wavelengths around 0.91 μm and 0.94 μm, these wavelengths being indicated by the arrows. Table 8 shows the derivation of the photon outputs of the two LED's. This method gave I_o values in fair agreement with I_o's calculated from the I_b measurements, using the absorption coefficient estimated for the LED in use. As before, unless the spacings, LED's, etc., were maintained constant, it was necessary to recalculate the I_o value for each different series of measurements.

For comparison, for the 0.91 μm LED, the value of I_o/α obtained for the EV samples was 5.2 $\mu A \cdot cm$ as shown in Table 5. Using the I_o value derived in Table 8 (890 μA) and the effective α-value from Table 7 (254 cm^{-1}) gives $I_o/\alpha \approx 3.5\,\mu A \cdot cm$. The errors in L-values measured by the I_b-method caused by this difference in I_o/α were $\sim$5% for $L \sim 65\,\mu m$, increasing to $\sim$15% for $L \sim 110\,\mu m$, and 20% for $L \sim 130\,\mu m$.

(c) Use of SPV Method instead of EV Method

Although preliminary measurements with the SPV method did not show good consistency, the promising results obtained by NASA-Lewis groups suggest that future work

in measuring L-values should re-evaluate the SPV method both as the main measurement method, and also for calibration purposes.

(d) Use of Samples Containing a Step

These samples have a step formed on the back surface, giving two regions of different base widths, W_1, W_2. Figure 28 shows such a sample. The back currents measured for the two sides of the steps are I_{b1} and I_{b2}.

By (B1),

$$I_{b1} = \frac{I_o}{\alpha W_1} \frac{\left(\frac{W_1}{L}\right)}{\text{Sinh}\left(\frac{W_1}{L}\right)} = \frac{I_o}{\alpha L} \frac{1}{\text{Sinh}\left(\frac{W_1}{L}\right)} \qquad \text{(B6)}$$

Similarly,

$$I_{b2} = \frac{I_o}{\alpha L} \frac{1}{\text{Sinh}\left(\frac{W_1}{L}\right)}$$

The ratio

$$\frac{I_{b2}}{I_{b1}} = \frac{\text{Sinh}\left(\frac{W_1}{L}\right)}{\text{Sinh}\left(\frac{W_2}{L}\right)} \qquad \text{(B7)}$$

Usually four iterations were sufficient to derive L in this equation. L could also be obtained from the ratio $\frac{I_{b2}}{I_{b1}}$ by using the fact that the sinh ratio is approximately $\exp \frac{(W_1-W_2)}{L}$. Thus measurement of the current ratio, and the step height (W_1-W_2), allows solution for L. In principle, this method offers the most direct way to derive L-values which can be used for calibration purposes.

If the assumption is made that L is constant across the sample containing a step (an assumption well justified from supporting checks of both I_b and I_f taken across the sample), the solution given is independent of the exact photon output and effective absorption coefficient. In practice, however, L-values obtained on step samples did not agree closely with measurements made using the EV samples for calibration.

An example of such inconsistency is given below.

A step sample gave the following measurements for the two sides of the step:

$$I_{b1} = 30\ \mu A, \qquad I_{b2} = 37\ \mu A,$$
$$W_1 = 528\ \mu m, \qquad W_2 = 422\ \mu m.$$

Using

$$\frac{I_o}{\alpha} = 5.2\ \mu A \cdot cm \text{ (from EV samples, Table 5)}$$

$$I_{b1} = \frac{I_o}{\alpha W_1} \cdot \frac{\left(\frac{W_1}{L}\right)}{\sinh\left(\frac{W_1}{L}\right)}$$

Using the values given,

$$\frac{\sinh\left(\frac{W_1}{L}\right)}{\left(\frac{W_1}{L}\right)} = 3.27$$

$$\therefore \frac{W_1}{L} = 2.98$$

$$\therefore L = 176\ \mu m.$$

Similar calculation for I_{b2}, W_2 gives

$$L = 139\ \mu m.$$

Using the step formula

$$\frac{I_{b2}}{I_{b1}} = \frac{\sinh\left(\frac{W_1}{L}\right)}{\sinh\left(\frac{W_2}{L}\right)} \approx \exp\frac{(W_1-W_2)}{L} \qquad \text{(B8)}$$

$$\Delta W = W_1 - W_2 = 106\ \mu m.$$

$$\therefore L = \frac{\Delta W}{\ln \frac{I_{b2}}{I_{b1}}} \approx 506\ \mu m.$$

The reason for this inconsistency was not found.

(e) Use of Ingots with High L-values

Ingots 973-8 and 9 were used. For L-values $\gtrsim 1000\ \mu m$, in equation (B3), $\alpha L \gg 1$ and the measured front current

$$I_f = I_o ; \qquad \text{(B9)}$$

in equation (B1), for small W, $\frac{W}{L}$ is small, and $\frac{\sinh\left(\frac{W}{L}\right)}{\left(\frac{W}{L}\right)} \to 1$ Thus,

$$I_b \approx \frac{I_o}{\alpha W} \qquad \text{i.e., } I_o = I_b \cdot \alpha W \qquad \text{(B10)}$$

In addition to this limiting condition for reasonably thin samples with high L-values, another check was obtained by measuring a series of samples of increasing thickness. These ingots were sliced to give a series of samples of increasing thickness. One group of such samples had a Schottky collecting barrier applied, and the other group was diffused. Back current L-measurements were made on both series of samples; front current L-measurements were also made on the diffused group.

The current measurements made on the samples from ingot 973-9 are shown in Table 10. These results are now analyzed in several different ways.

(i) Using the $\frac{I_o}{\alpha}$ value obtained from EV calibration

$\frac{I_o}{\alpha} = 5.2\ \mu A \cdot cm$ (from Table 5)

Table 11 shows the L-values calculated from the I_b values in Table 10.

(ii) Using equation (B10) for the thinnest sample, (#1)

$\frac{I_o}{\alpha} = 1.4\ \mu A \cdot cm$

Using this value for samples 2 through 6 gives the L-values shown in Table 12. These values differ from those in Table 11 (much higher).

(iii) Using measurements for successive samples

Assuming L is the same for two samples of successive thickness, L can be obtained by taking the I_b ratio for the two samples.

For example, for samples #4 and #5 in Table 10.

Let $\frac{W_4}{L} = x_4$, $\frac{W_5}{L} = x_5$.

$$\frac{I_{b4}}{I_{b5}} = \frac{\sinh x_5}{\sinh x_4} = \varepsilon^{(x_5 - x_4)} \left[\frac{1 - \exp(-2x_5)}{1 - \exp(-2x_4)}\right] \quad \text{(B11)}$$

Assume the $\left[\frac{1 - \exp(-2x_5)}{1 - \exp(-2x_4)}\right]$ term = 1.

From (B10),

$L = 1074^{*}\ \mu m \qquad 1698^{+}\ \mu m.$

Iteration 1 Using these L-values in equation (B11), solving for L gives,

$L = 1140^{*}\ \mu m \qquad 2238^{+}\ \mu m.$

* refers to undiffused samples.

\+ refers to diffused samples.

Iteration 2 Using L-values from iteration 1, in (B11), gives

$L = 1152^{*}\ \mu m \qquad 2590^{+}\ \mu m.$

Iteration 3 Using L-values from iteration 2, in (B11), gives

$L = 1155^{*}\ \mu m \qquad 2860^{+}\ \mu m.$

The values obtained for the undiffused samples are close to those shown in Table 12.

However, the values for the diffused samples differ widely.

The differences between the values obtained in (iii) and (i) are similar to the inconsistencies obtained on the step samples ((d) above).

(iv) Graphical Representation

Equation (B1) may also be written as (B6), namely,

$$I_b = \frac{I_o}{\alpha L} \frac{1}{\sinh\left(\frac{W}{L}\right)} \qquad (B6)$$

Assume L is constant for all samples.

Then $I_b = k_1 \frac{1}{\sinh\left(\frac{W}{L}\right)}$ where $k_1 = \frac{I_o}{\alpha L}$.

(α) Assume further that $\frac{W}{L}$ is small.

Then $\sinh\left(\frac{W}{L}\right) \rightarrow \left(\frac{W}{L}\right)$.

$$I_b = \frac{k_1}{\frac{W}{L}} = \frac{k_2}{W} \qquad \text{where } k_2 = k_1 L = \frac{I_o}{\alpha}.$$

A plot of ln I_b versus ln W would be a straight line with a slope = -1. Figure 29 shows such a plot for the samples of 973-9. For $W < 1250\ \mu m$, the slope is

* refers to undiffused samples.

\+ refers to diffused samples.

close to -1. (i.e., since $\frac{W}{L}$ is small, this implies an L-value $\gtrsim$ 1000 μm.)

(β) For the other extreme, assume that $\frac{W}{L}$ is large.

Then $\sinh\left(\frac{W}{L}\right) \rightarrow \frac{\varepsilon^{\left(\frac{W}{L}\right)}}{2}$.

Thus (B6) becomes $I_b = \frac{I_o}{L} \frac{2}{\varepsilon^{\left(\frac{W}{L}\right)}} = \frac{k_3}{\varepsilon^{\left(\frac{W}{L}\right)}}$ where $k_3 = \frac{2I_o}{\alpha L}$.

A plot of ln I_b versus W would give a straight line of slope $-\frac{1}{L}$. Figure 30 shows the plot. The values for L derived from the slope of this plot approaches those obtained in (ii) above. This approximation has the disadvantage that the I_b measurements which are most critical for determining L are those for the thicker samples where the I_b-values are very low.

The fact that back currents were measured (even very low values) as a result of minority carriers moving through large thicknesses (up to 350 mils) of silicon, supports the long lifetime measurements made by the vendor.

B.2.6 Other Comments on PV Method

Several other tests were made on the experimental assumptions underlying the PV method.

First, transmission comparison made on samples with or without the diffused N+ layer, using the low α light sources used for I_f-measurements showed that no measurable absorption was occurring in the N+ layer. This agrees with numerical estimates. Second, transmission tests on

silicon slices of varying resistivity showed that the effective α-value increased slightly as the resistivity of the silicon decreased. These slight α-variations would require adjustments in the calculations if greater accuracy in PV L-measurements was required.

B.3 Summary of the Photovoltaic Method

The PV method provided a convenient way to characterize a wide variety of ingots. The method showed good repeatibility for samples, and good consistency for several samples from the same ingot. Table 9 shows the good consistency obtained. This table also shows that there was some difference ($\sim$25%) in the L-values obtained by the I_b and I_f methods. This is thought to be due to slight differences in the analytical assumptions made. For higher L-values ($> 90\ \mu m$) the I_b-values of L are thought to be more accurate because the assumptions were better. For L-values below $90\ \mu m$, the I_f-values are probably more accurate. More work is needed to explain the inconsistencies in step samples (d) and long L-ingots (e). With these stated limitations, the general level of accuracy compared well with earlier diffusion length or lifetime measurements, particularly when the large range of resistivity and diffusion lengths is considered.

TABLE 1

Ingot Details*

Ingot	Supplier	Method of Growth	Resistivity (ohm-cm)	Oxygen Conc. (cm^{-3})	Etch Pit Density (cm^{-3})	Comments
973- 1	Dow Corning	Crucible	0.1	$>10^{17}$	$>10^{4}$	
973- 2	Dow Corning	Crucible	0.1	$>10^{17}$	$\rightarrow 0$	
973- 3	Dow Corning	Vac Float Zone	0.1	$<2 \times 10^{15}$	$>3 \times 10^{4}$	
973- 4	Dow Corning	Vac Float Zone	0.1	$<2 \times 10^{15}$	$>2 \times 10^{4}$	Extra pure
973- 5	Dow Corning	Vac Float Zone	0.1	$<10^{16}$	$\rightarrow 0$	Additional dislocation-free pass
973- 6	Dow Corning	Crucible	7	$>10^{17}$	$\sim 10^{4}$	
973- 7	Dow Corning	Crucible	8.5	$>10^{17}$	$\rightarrow 0$	
973- 8	Dow Corning	Vac Float Zone	10.5	$<2 \times 10^{15}$	$>2 \times 10^{4}$	
973- 9	Dow Corning	Vac Float Zone	9	$<10^{17}$	$\rightarrow 0$	Additional dislocation-free pass
973-10	Centralab	Crucible	0.01	$>10^{17}$	$>10^{4}$	
973-11	Centralab	Crucible	0.01	$>10^{17}$	$<10^{3}$	
973-12	Texas Inst.	Lopex	0.01	$<10^{16}$	$\rightarrow 0$	
973-13	Centralab	Crucible	1.0	$>10^{17}$	$>10^{4}$	
973-14	Centralab	Crucible	1.0	$>10^{17}$	$<10^{3}$	
973-15	Texas Inst.	Lopex	1.0	$<10^{16}$	$\rightarrow 0$	
973-16	Wacker	Waso	1.0	$<10^{16}$ (?)	$\rightarrow 0$	
973-17	Wacker	Waso	0.05	$<10^{16}$ (?)	$\rightarrow 0$	

* All ingots were P-type, boron-doped, grown in (111) direction and sliced perpendicular to growth axis.

TABLE 2

Cell Processing Sequence

Step Identification Number	Operation	Typical Temperature °C
I	Ingot sliced	
	Mount slices on plate	
	Slices lapped (one side)	
	Slices polished (one side)	~25 (and localized heating in grinding)
	Remove from plate	
	Clean	
II	Light chemical etch	
	Phosphorous diffusion	~900
III	Anneal	~860
IV	Protect polished surface	
	Sandblast and/or light etch to remove N+ layer on back	
	Remove diffusion glass	
	Clean for evaporation	~50
	Evaporate metal contacts (front and back)	
V	Evaporate antireflective coating	~25
VI	Sinter	~600
	Edge etch*	~25

* If processing ended at stages IV or V, this etch was performed.

TABLE 3

Etch Pit Densities (cm^{-3})

Ingot No.	Goal	Vendor Measurement	CRL Measurement	
			Before Diff.	After Diff.
973- 1	$>10^4$	1.1×10^4	3×10^3	3×10^3
973- 2	$<10^3$	$<10^3$	$<10^3$	$<10^3$
973- 3	$>10^4$	3×10^4	3×10^4	15×10^4
973- 4	$>10^4$	2.5×10^4	15×10^4	14×10^4
973- 5	$<10^3$	$<10^3$	$<10^3$	$<10^3$
973- 6	$>10^4$	9×10^3	1.2×10^4	10^4
973- 7	$<10^3$	$<10^3$	$<10^3$	$<10^3$
973- 8	$>10^4$	2×10^4	---	---
973- 9	$<10^3$	$<10^3$	---	---
973-10	$>10^4$	---	$<10^3$*	$<10^3$*
973-11	$<10^3$	---	$<10^3$	$<10^3$
973-12	$<10^3$	$<10^3$	---	---
973-13	$>10^4$	---	5×10^3	2×10^3
973-14	$<10^3$	---	2×10^3	$<10^3$
973-15	$<10^3$	$<10^3$	10^4* ?	$<10^3$

* The values which did not meet the goal are marked with an asterisk.

TABLE 4

Saturation Current Densities (and V_{oc}) Calculations

N_A [a] cm^{-3}	D_n [b] cm^2/sec	τ_n [c] sec	J_{OD} [d] amp/cm^2	$(V_{oc})_D$ [e] mV	W [f] cm	τ_{DL} [g] sec	J_{OS} [h] amp/cm^2	$(V_{oc})_S$ [i] mV
1.5×10^{15}	35	1.1×10^{-5}	4.05×10^{-11}	535	8×10^{-5}	7.3×10^{-8}	1.27×10^{-6}	535
3×10^{16}	25	7×10^{-6}	2.1×10^{-12}	615	2.7×10^{-5}	4.65×10^{-8}	6.5×10^{-7}	570
7×10^{17}	11	9×10^{-6}	5.3×10^{-13}	650	10^{-5}	6×10^{-8}	1.93×10^{-7}	634
1.5×10^{18}	7.5	5.5×10^{-6}	2.6×10^{-14}	730	7×10^{-6}	3.65×10^{-8}	2.23×10^{-7}	625
3.5×10^{18}	3.5	5×10^{-8}	6.7×10^{-14}	705	5×10^{-6}	5.33×10^{-10}	1.08×10^{-5}	422

Notes:

a. Calculated from resistivity and capacitance measurements.

b. Using Irvin's mobility values[16].

c. Calculated from L-measurements.

d. $J_{OD} = \frac{qn_i^2}{N_A} \cdot \sqrt{\frac{D_n}{\tau_n}}$

e. $V_{oc} = 60 \log\left(\frac{0.035}{J_{OD}}\right)$

f. From capacitance measurements.

g. Assuming $\tau_{DL} = \frac{1}{150} \tau_n$

h. $J_{OS} = \frac{qn_i}{2} \cdot \frac{W}{\tau_{DL}}$

i. $V_{oc} = 120 \log\left[\frac{0.035}{J_{OS}}\right]$

TABLE 5

Electronvoltaic Diffusion Length

Calibration Samples for I_b Method

Cell No.	Thickness W, μm	Diffusion Length* L, μm	$\frac{W}{L}$	$\frac{\sinh\left(\frac{W}{L}\right)}{\left(\frac{W}{L}\right)}$	I_b + (μA)	$\frac{I_o}{\alpha}$ (μA·cm)
2	387	112	3.44	4.5	31	5.4
20	405	165	2.45	2.35	51	4.8
21	387	133	2.7	2.72	50	5.3
22	403	162	2.48	2.39	55	5.3
19	378	139	2.72	2.76	49.5	5.15
						5.2 avg

* Measured by electronvoltaic method at TRW Systems.

\+ Back current PV reading using LED, $\lambda \approx 0.91$ μm.

TABLE 6

Electronvoltaic Diffusion Length Calibration Samples for I_f Method

Cell No.	Thickness W, μm	I_f + (μA)	Diffusion Length* L, μm	αL □	1+(αL)	I_o (μA)
1 - VI - 1	320	113	21	.022	1.022	5250
3 - VI - 3	311	242	73	.076	1.076	3430
4 - VI - 1	324	186	43	.045	1.045	4319
5 - VI - 3	322	297	59	.061	1.061	5166
6 - VI - 3	661	431	185	.192	1.192	2676
Test 15, #6	305	281	102	.106	1.106	2932

* Measured by electronvoltaic method at TRW Systems

\+ Forward current PV reading, using tungsten lamp + 1.06 μm filter (+ 10 mils silicon)

□ Calculated using $\alpha = 10.4\ cm^{-1}$

TABLE 7

Measured Absorption Coefficient (α) for Four Light Sources Used for PV Method

Light Source	Effective α, cm^{-1}
LED, $\lambda \approx 0.91$ μm	254
LED, $\lambda \approx 0.94$ μm	154
Tungsten lamp + 1.06 μm filter (+ 10 mils silicon)	10.4
Tungsten lamp + 190 mils silicon	2

TABLE 8

Calculation of the Photon Current of an LED

Using a Calibrated Photocell*

Quantity	Light Sources	
	LED 1	LED 2
Current in LED (mA)	40	40
Wavelength of LED (λ, μm)	0.91	0.94
Current generated in cell 2A-4B (I_{sc}, μA)	670	1216
Cell response at output λ (R, μA/μW)	0.545	0.545
Power output from LED (P) is given by $P = \frac{I_{sc}}{R}$ (μW)	1229	2231
Energy per photon at λ (E, eV)	1.36	1.316
Number of photons per second output (ϕ, sec^{-1}) $\phi = \frac{P}{E} = \frac{P \text{ (watts)}}{E \text{ (eV)} \times 1.6 \times 10^{-19}}$	5.64×10^{15}	1.06×10^{16}
Current output (I_o) $I_o = q\phi = 1.6 \times 10^{-19}\phi$ (A) $= 1.6 \times 10^{-13}\phi$ (μA)	902 μA	1694 μA

* Cell 2A-4B was used; its absolute spectral response is shown in Figure 27.

TABLE 9

I_b and I_f L-measurements on Several Samples to Show Repeatibility

Ingot	Sample No.	Resistivity ohm-cm	W μm	I_b* μA	L μm	I_f+ μA	L μm
973-16 Undiffused	1	1	323	47.5	108	not measured	
	2		343	45.	114		
	3		327	45.	106		
	4		332	47.5	111		
973-16 Diffused	1	1	374	36.	116	840	67
	2		386	36.5	122	1099	125
	3		389	37.5	125	1057	114
	4		379	40.	124	1048	112
	5		380	33.	115	1032	107
	6		382	33.	115	not measured	
	7		379	34.5	115		
	8		379	35.	116		
973-17 Undiffused	1	0.05	312	12.5	64.	not measured	
	2		305	12.0	61.5		
	3		305	12.5	62.		
	4		318	12.0	65.		
973-17 Diffused	1	0.05	---	2.5	---	709	48.6
	2		368	5.2	64.	778	57.5
	3		368	4.6	62.5	742	52.5
	4		365	4.3	61.	756	54.5
	5		368	4.2	61.5	763	55.5
	6		365	4.5	61.5	770	56.5
	7		370	4.2	61.5	754	54.3
	8		375	4.0	62.	765	55.7
	9		368	4.5	62.	762	55.5
	10		378	3.8	60.5	726	50.5

* Using LED, $\lambda \sim 0.91$ μm.

\+ Using LED, $\lambda \sim 0.94$ μm.

TABLE 10

I_b Measurements for Thick Samples from Ingot 973-9 (Long Diffusion Length)

Sample No.	Undiffused Samples		Diffused Samples	
	Thickness W, μm	I_b * μA	Thickness W, μm	I_b * μA
1	389	36	326	44.6
2	653	20	660	23
3	1207	10	1176	12.4
4	1684	6.2	1636	7.2
5	2210	3.8	2154	5.3
6	8800	0.1	8820	0.09

* Using light source, LED, $\lambda \sim 0.91$ μm.

TABLE 11

Calculated Diffusion Lengths in Thick Samples from Ingot 973-9

Sample Number	Thickness μm	Undiffused Samples		Diffused Samples	
		I_b μA	L* μm	I_b μA	L* μm
1	389	36	123	44.6	104
2	653	20	195	23	218
3	1207	10	355	12.4	380
4	1684	6.2	475	7.2	476
5	2210	3.8	575	5.3	625
6	8800	0.1	2330(?)	0.09	1300

Notes Used LED with $\lambda = 0.91\ \mu$m.

* Calculated using $\frac{I_o}{\alpha} = 5.2\ \mu A \cdot cm$.

TABLE 12

Calculated Diffusion Lengths in Thick Samples from Ingot 973-9

Sample Number	Thickness μm	Undiffused Samples		Diffused Samples	
		I_b μA	L* μm	I_b μA	L* μm
1	389	36	7700(?)	44.6	--
2	653	20	1010	23	--
3	1207	10	1270	12.4	--
4	1684	6.2	1220	7.2	1560
5	2210	3.8	1190	5.3	1930
6	8800	0.1	1740	0.09	1680

Notes Used LED with $\lambda = 0.91\ \mu m$

* Calculated using $\frac{I_o}{\alpha} = 1.4\ \mu A \cdot cm.$

FIGURE 1

Diffusion Length vs. Resistivity (N-Si)

Ref: D. Kendall, NASA-GSFC X-711-69-366
(Conference on Lithium Diffused Silicon)

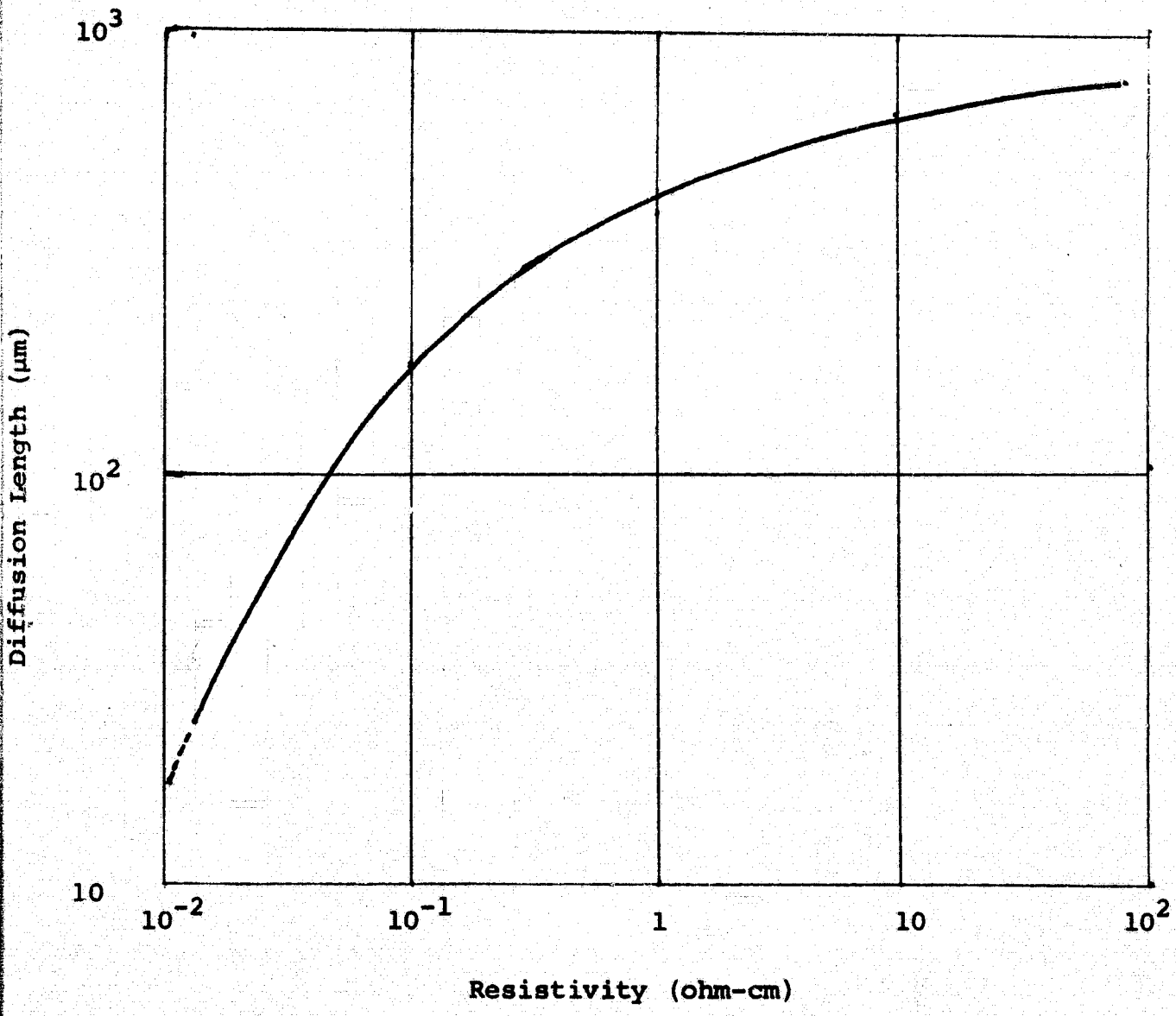

FIGURE 2

J_{sc} vs. L (10 ohm-cm N/P)

(from Ref. 4)

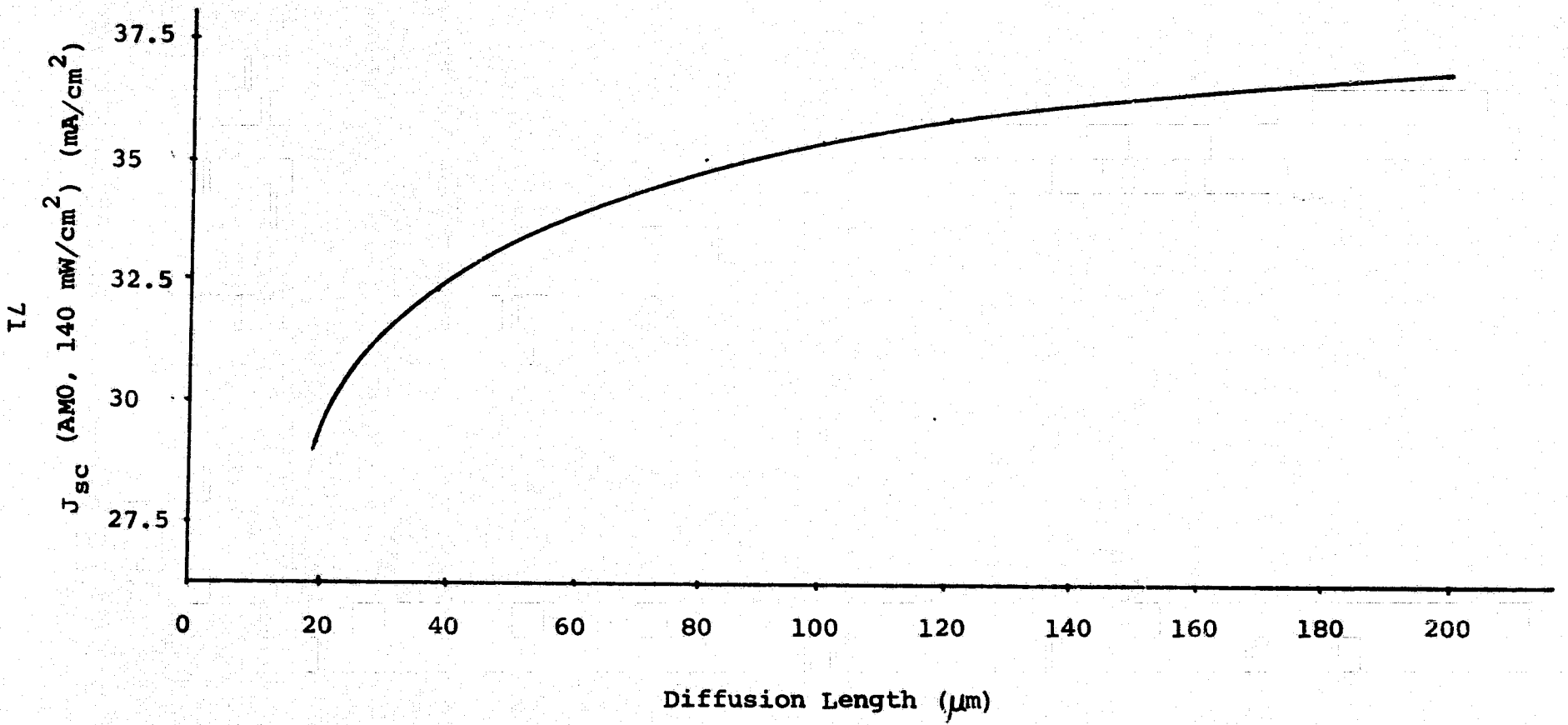

FIGURE 3

Short Circuit Current Density vs. Resistivity

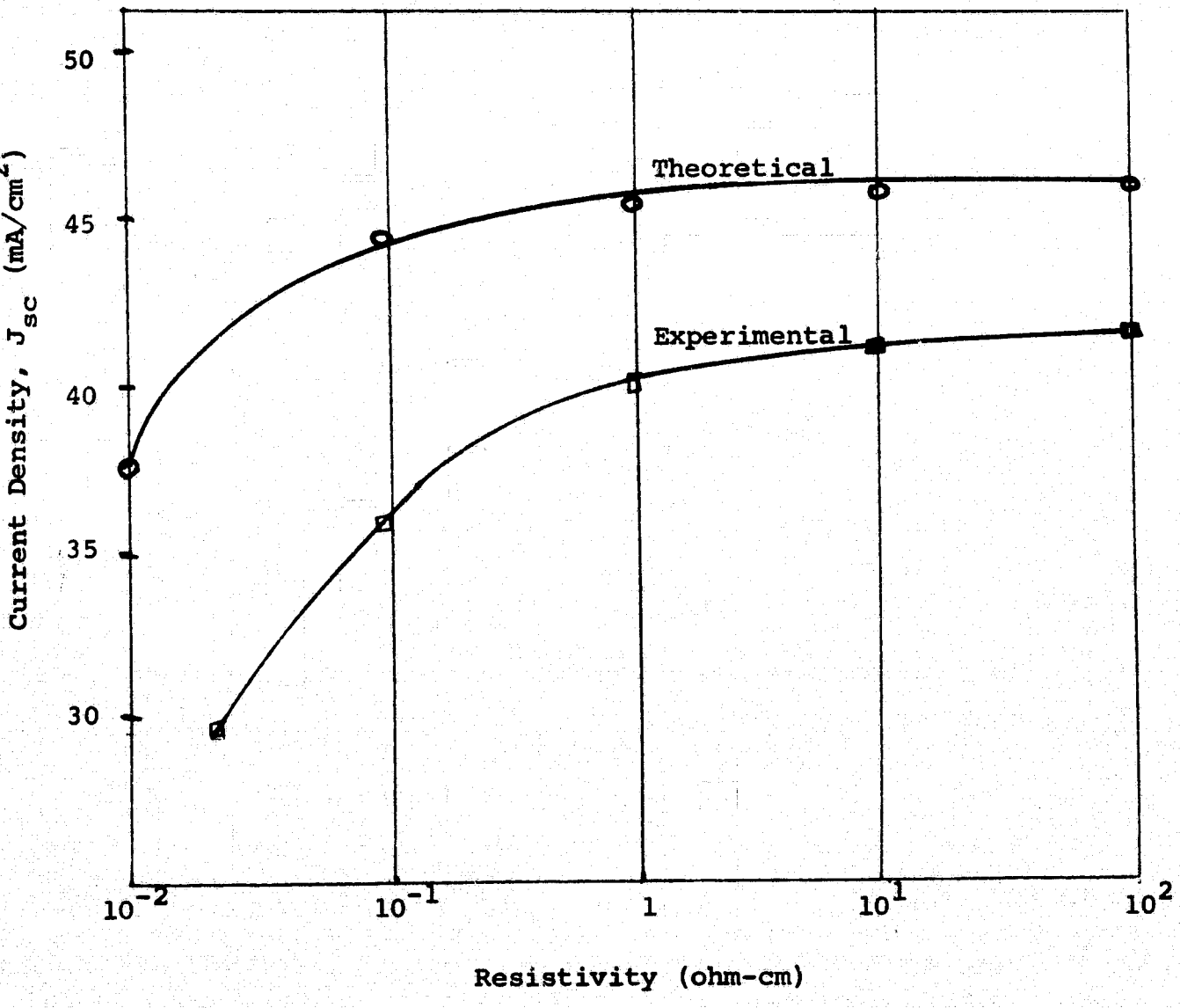

FIGURE 4

V_{OC} vs. Resistivity

Comparison of Theory and Experiment

(Ref. 2)

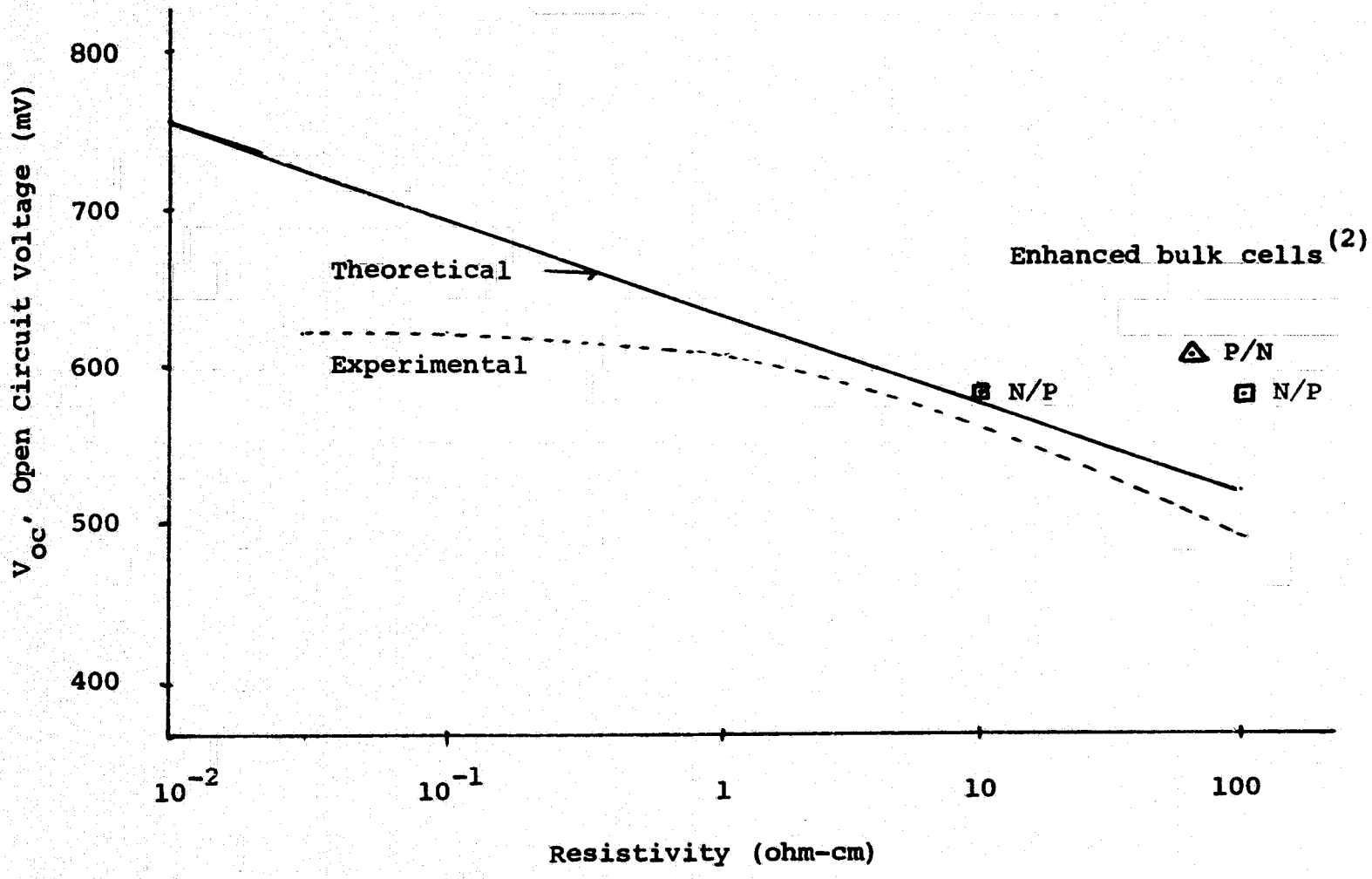

FIGURE 5

Sample Structures for PV L-measurements

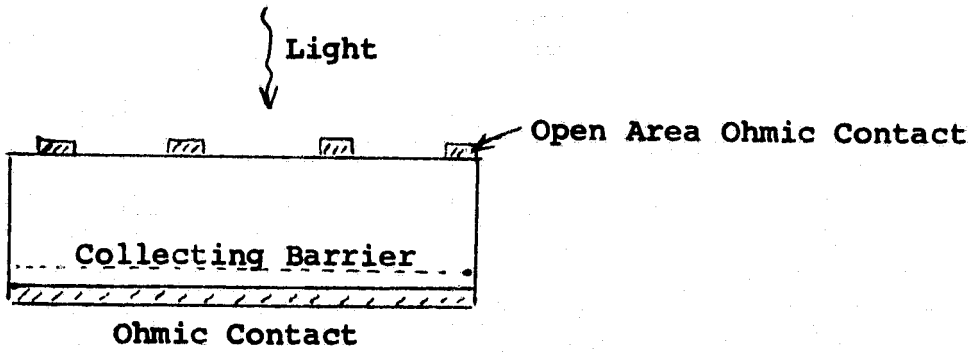

17(a) Back Current Method

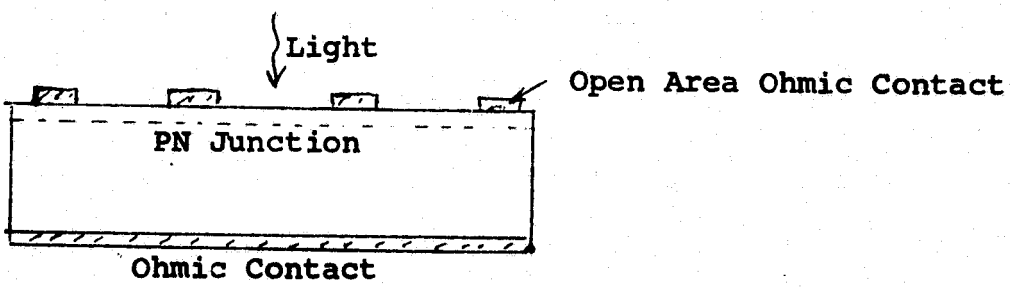

17(b) Front Contact Method

17(c) Open Area Contact Structures Used

FIGURE 6

Diffusion Length after Processing Steps

Ingots 973- (1 to 3)

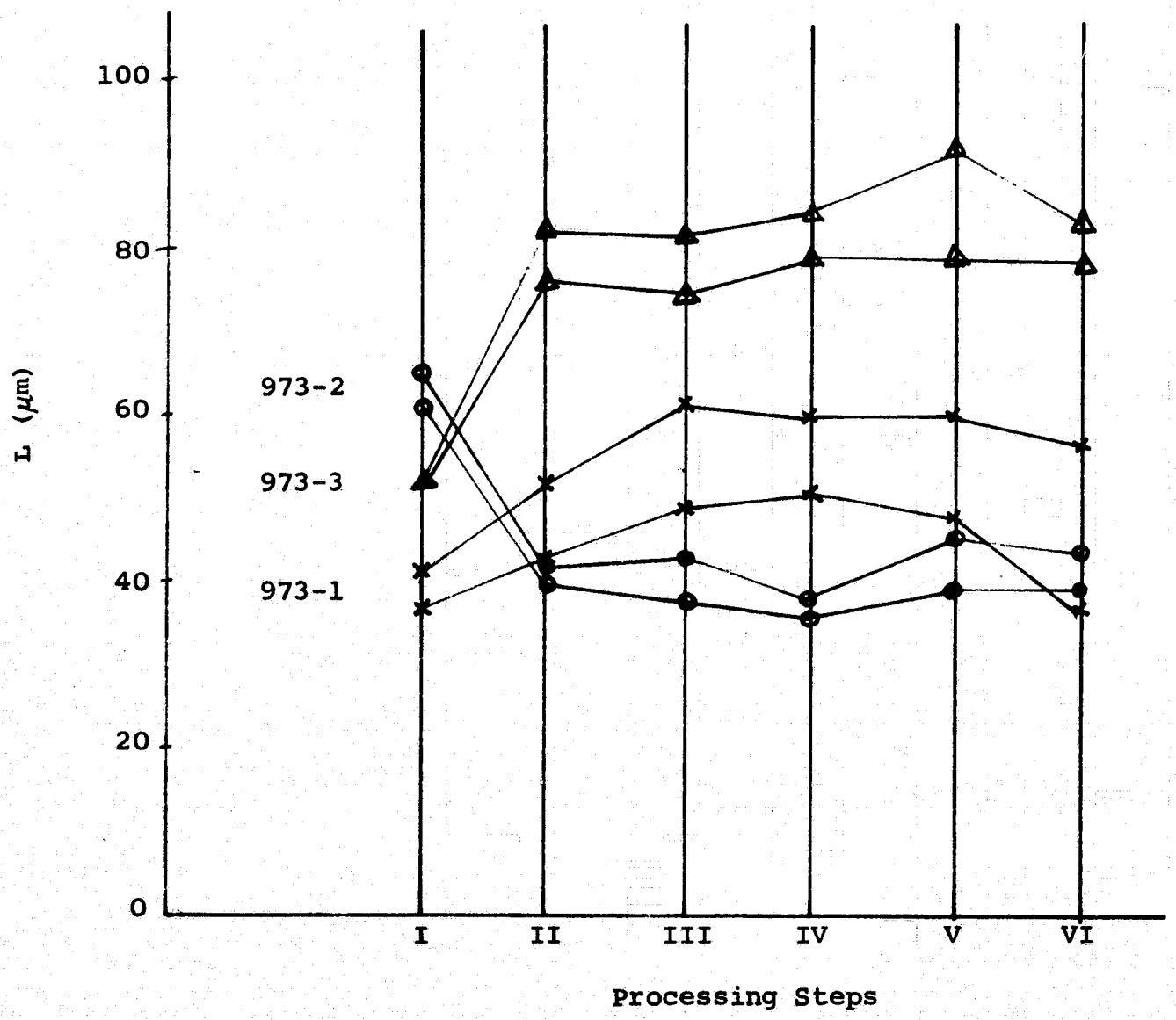

FIGURE 7

Diffusion Length after Processing Steps

Ingots 973- (4 to 7)

and 973-15

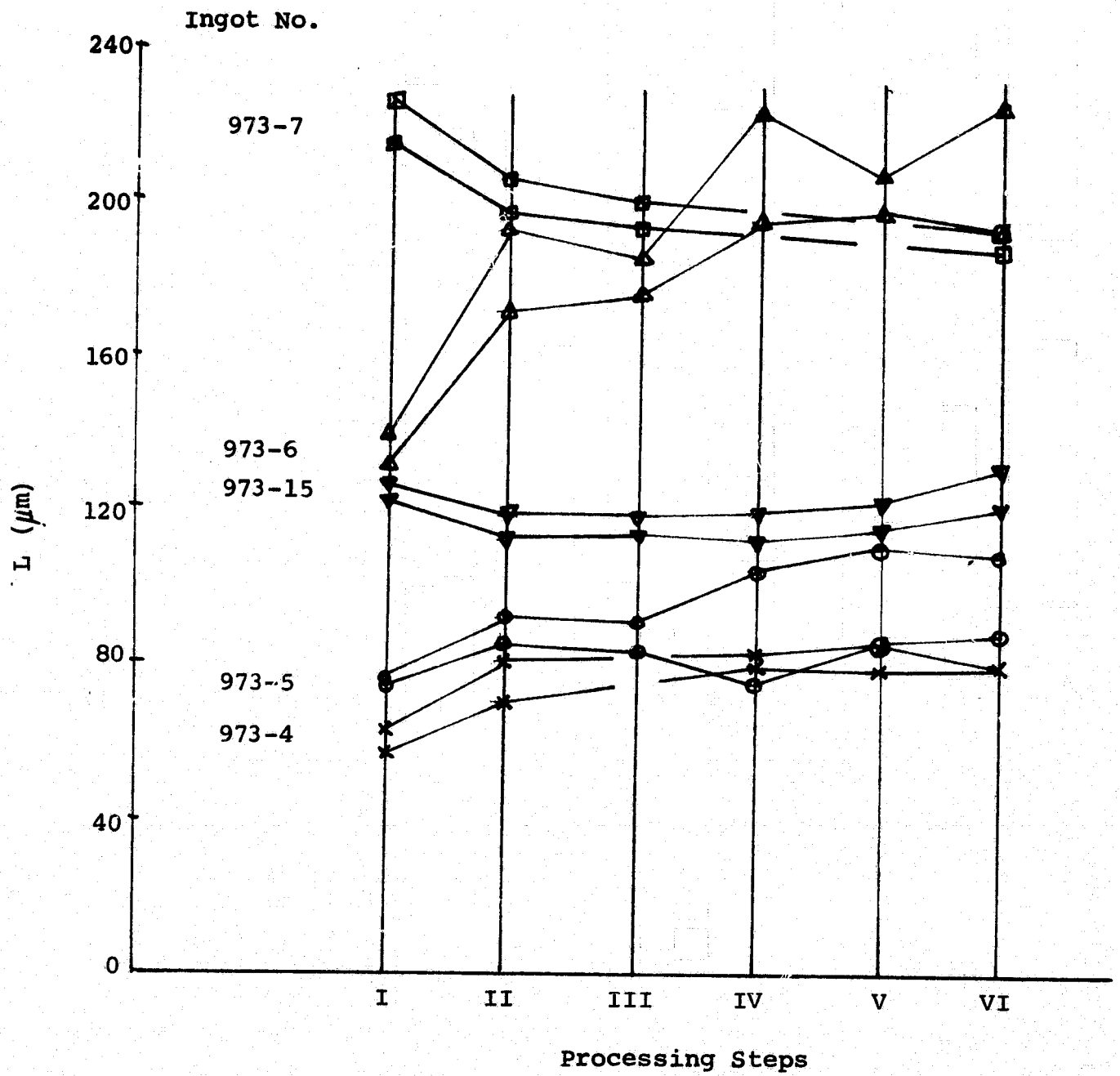

FIGURE 8

Diffusion Length after Processing Steps

Ingots 973- (10 to 12)

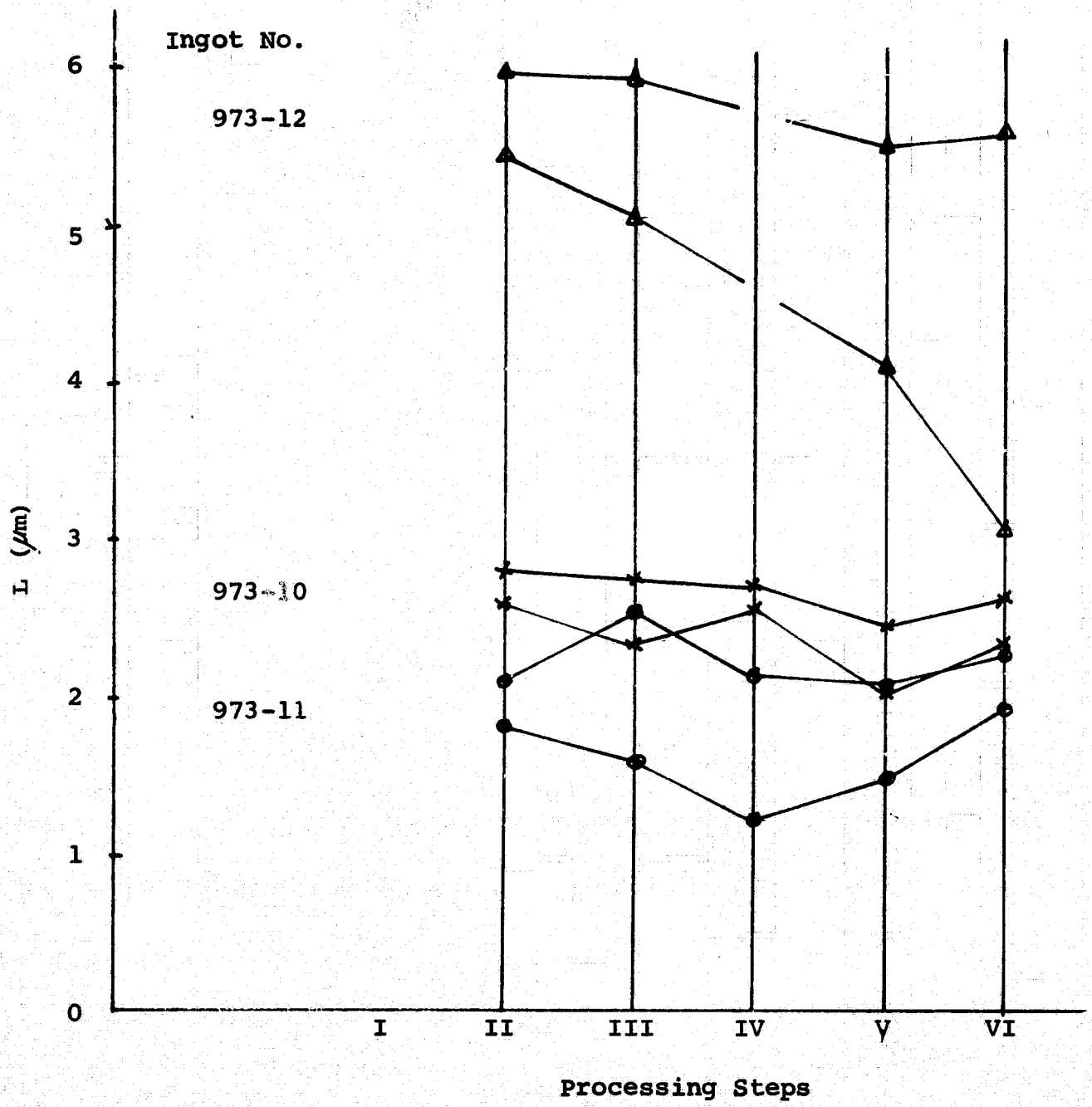

FIGURE 9

Diffusion Length after Processing Steps

Ingots 973- (13, 14, 16, 17)

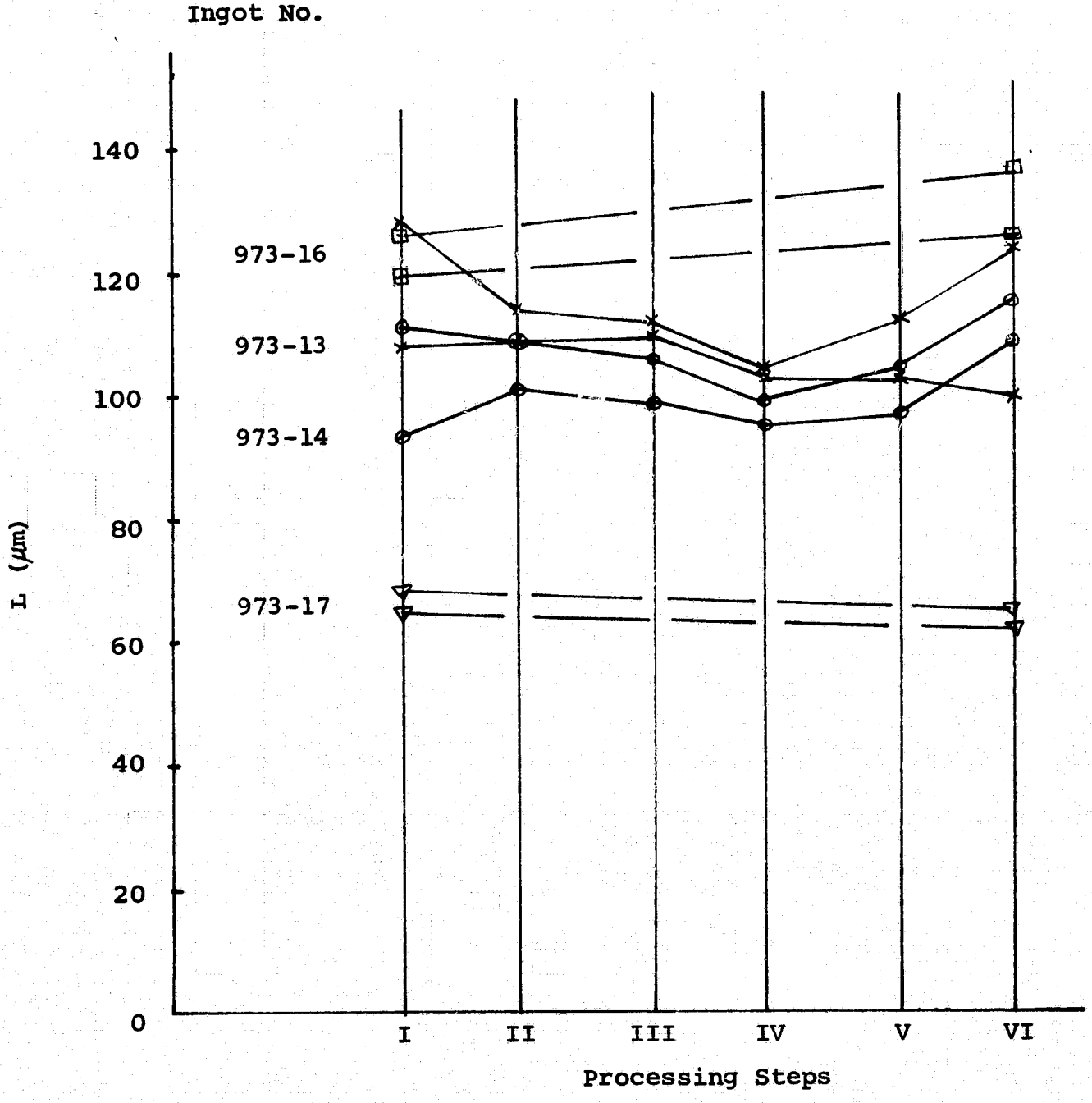

FIGURE 10

Diffusion Length after Various Processing Steps

LEGEND:

I	- after polishing	IV	- after contacts
II	- after diffusion	V	- after coating
III	- after annealing	VI	- after sintering

NOTE: Ingots 973-8,9 have L > 1000 μm at steps I and VI.

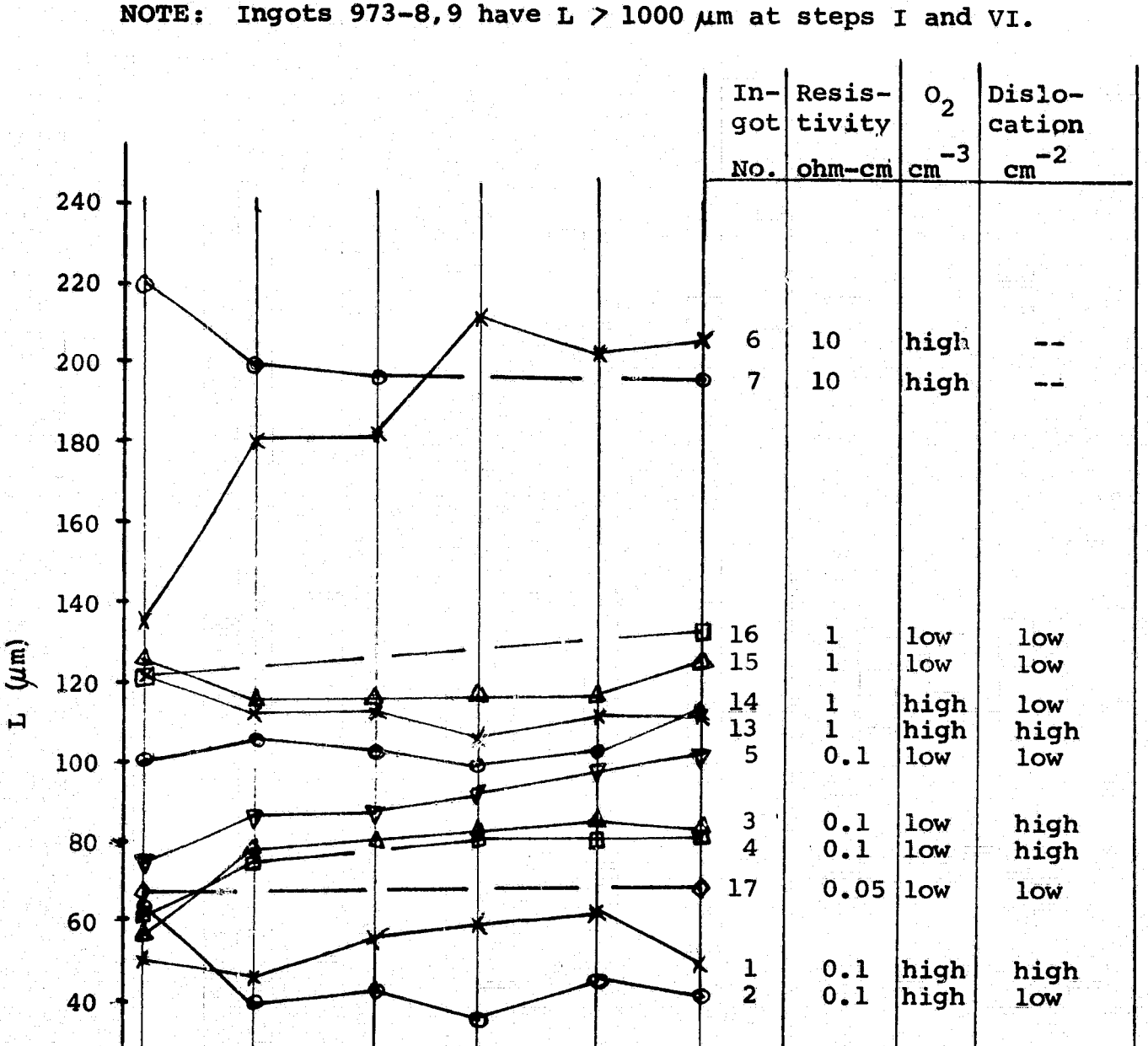

Ingot No.	Resistivity ohm-cm	O_2 cm^{-3}	Dislocation cm^{-2}
6	10	high	--
7	10	high	--
16	1	low	low
15	1	low	low
14	1	high	low
13	1	high	high
5	0.1	low	low
3	0.1	low	high
4	0.1	low	high
17	0.05	low	low
1	0.1	high	high
2	0.1	high	low
12	0.01	low	low
10	0.01	high	high
11	0.01	high	low

FIGURE 11

Diffusion Length vs. Resistivity

LEGEND: First letter - high or low O_2

Second letter - high or low dislocations

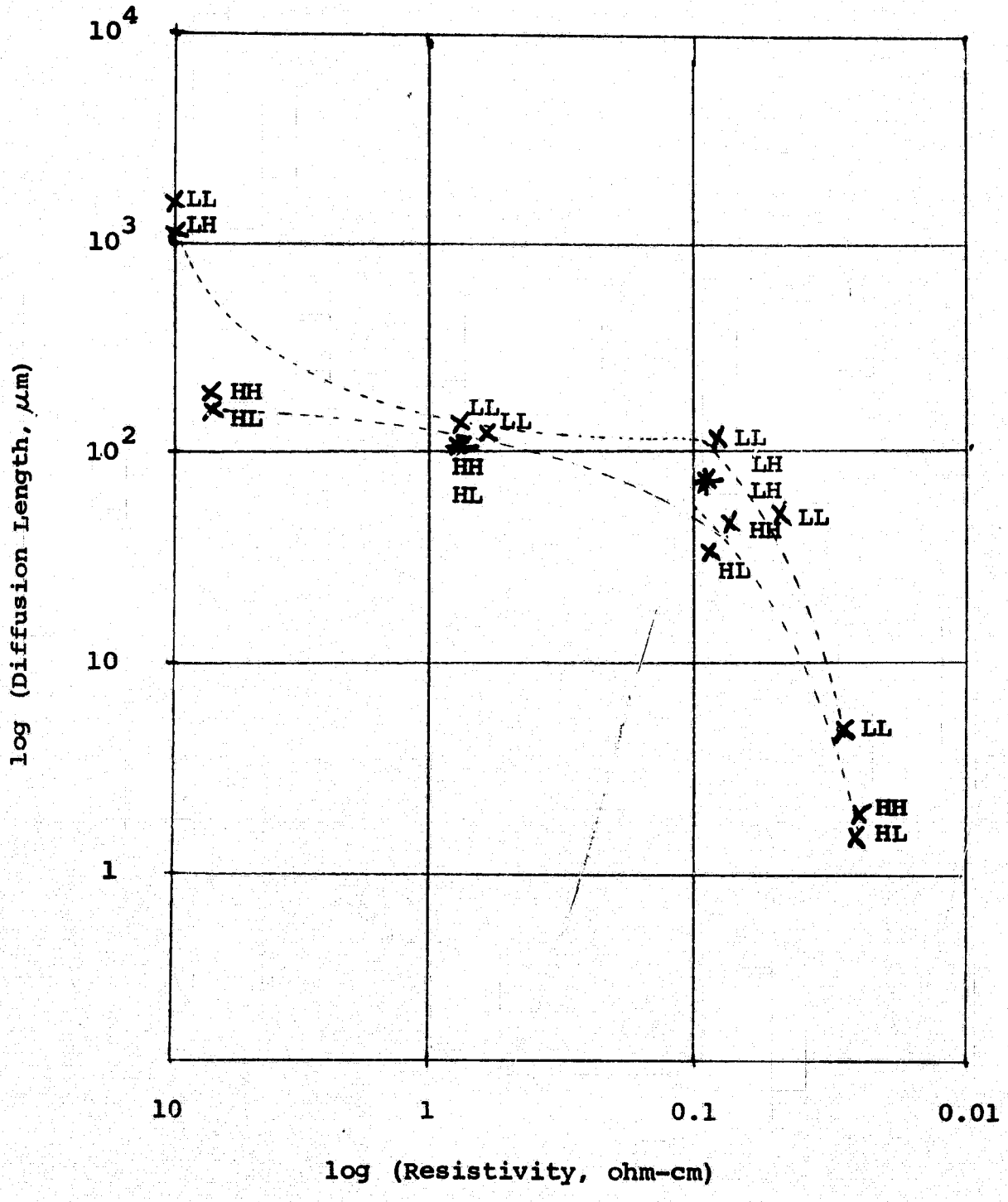

FIGURE 12

Diffusion Length vs. Acceptor Concentration

LEGEND: The first letter - high or low O_2

The second letter - high or low dislocation

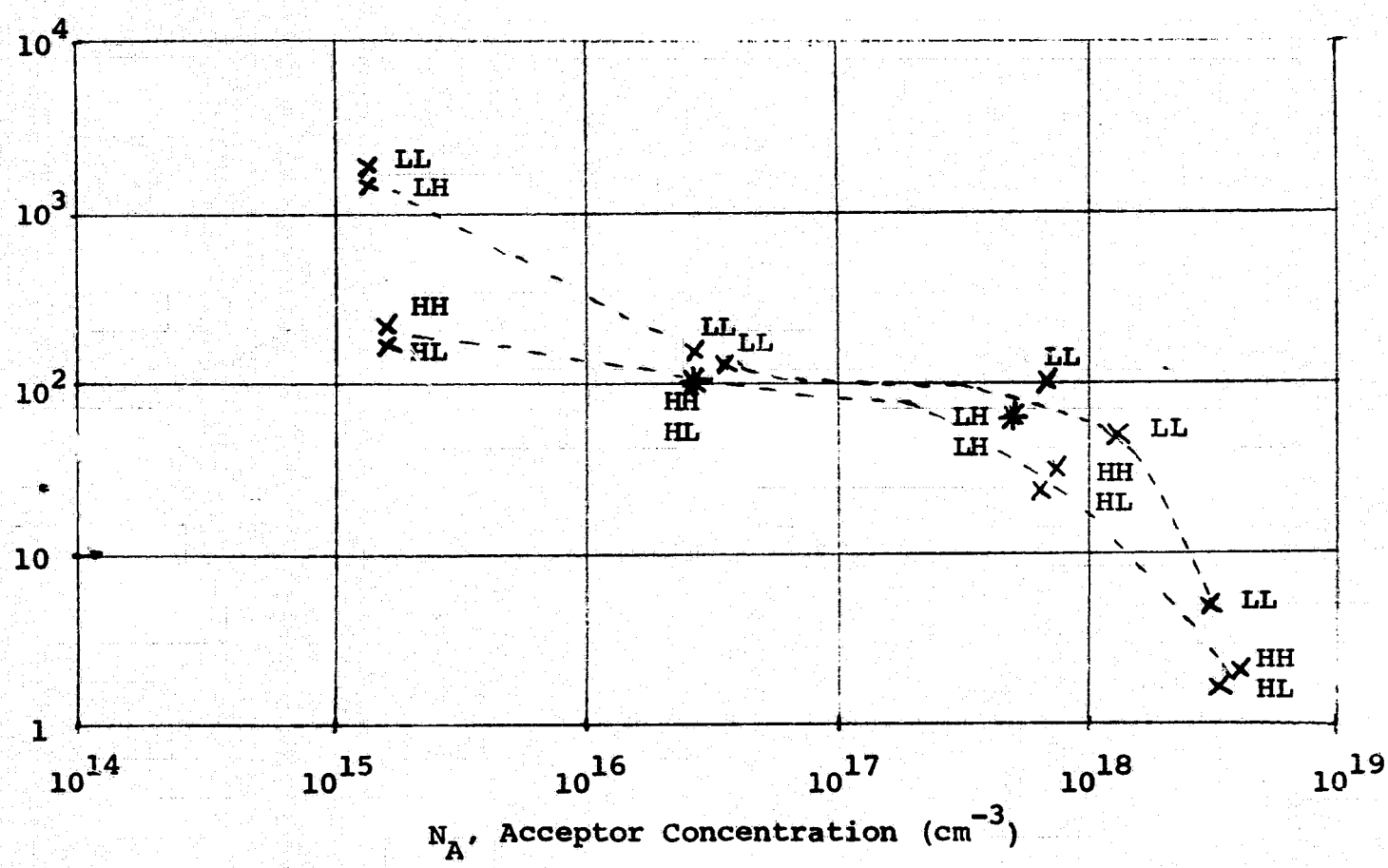

FIGURE 13

Minority Carrier Lifetime vs. Acceptor Concentration

LEGEND: Numbers are 973 ingot numbers.

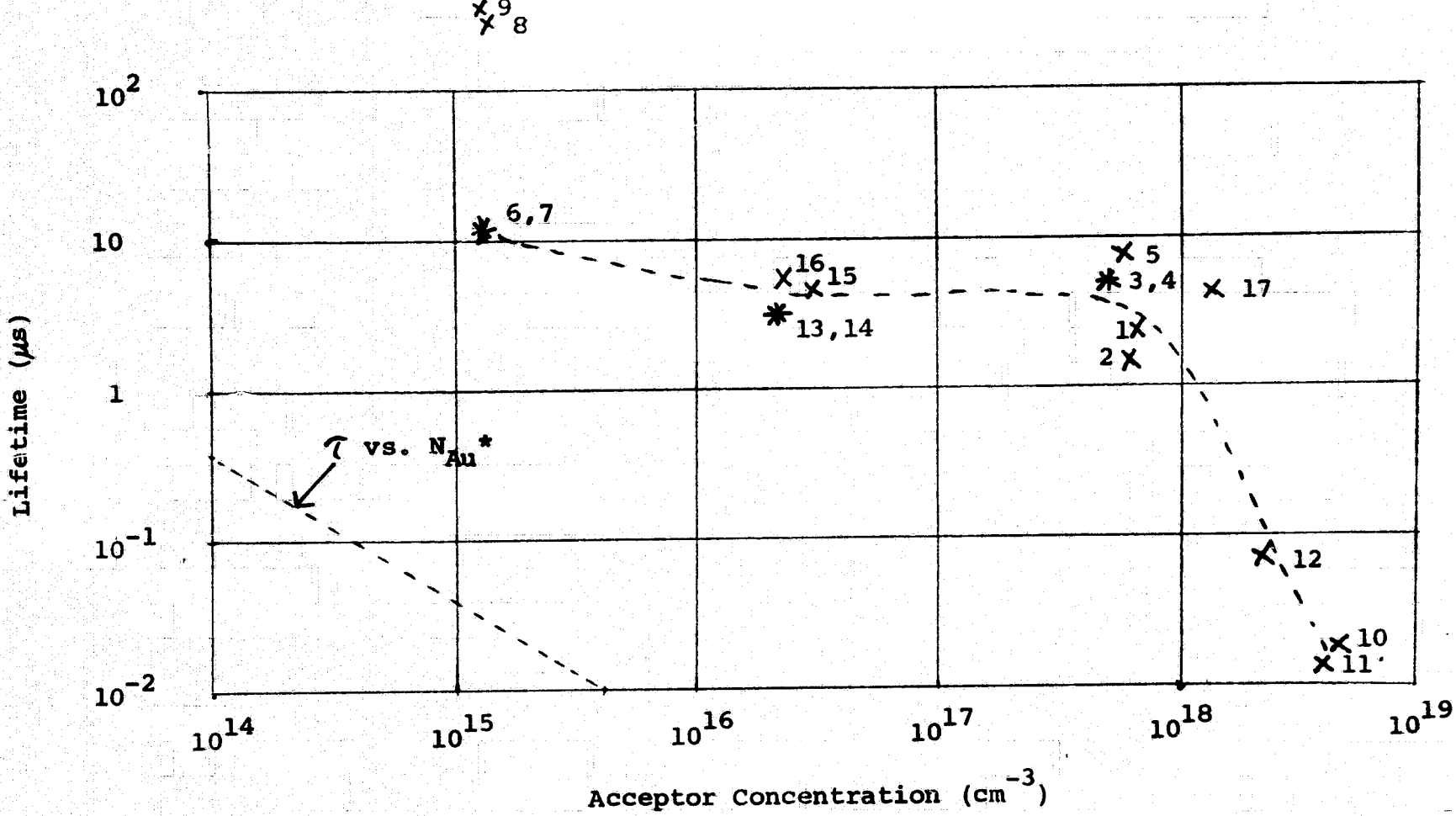

* For P-silicon, Fairfield, Gokhale, Solid State Electronics 9 1966, p. 905

FIGURE 14

I_{sc} (AM0) vs. N_A

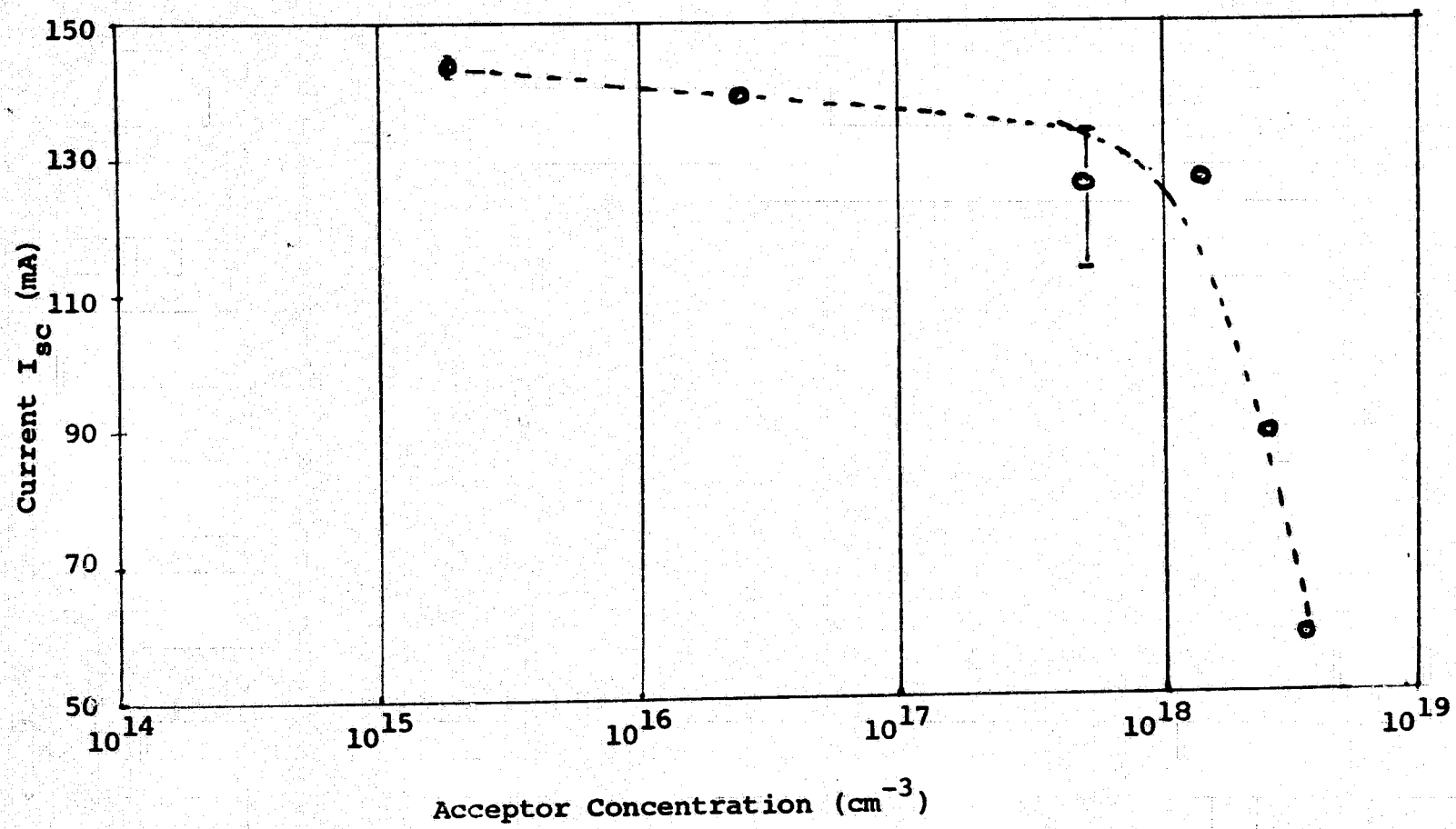

FIGURE 15

I_{sc} vs. Diffusion Length

LEGEND:

- □ - 10 ohm-cm (from Figure 1)
- o - 10 ohm-cm
- \+ - 1 ohm-cm
- x - 0.1 ohm-cm
- △ - 0.01 ohm-cm
- ▽ - 0.05 ohm-cm

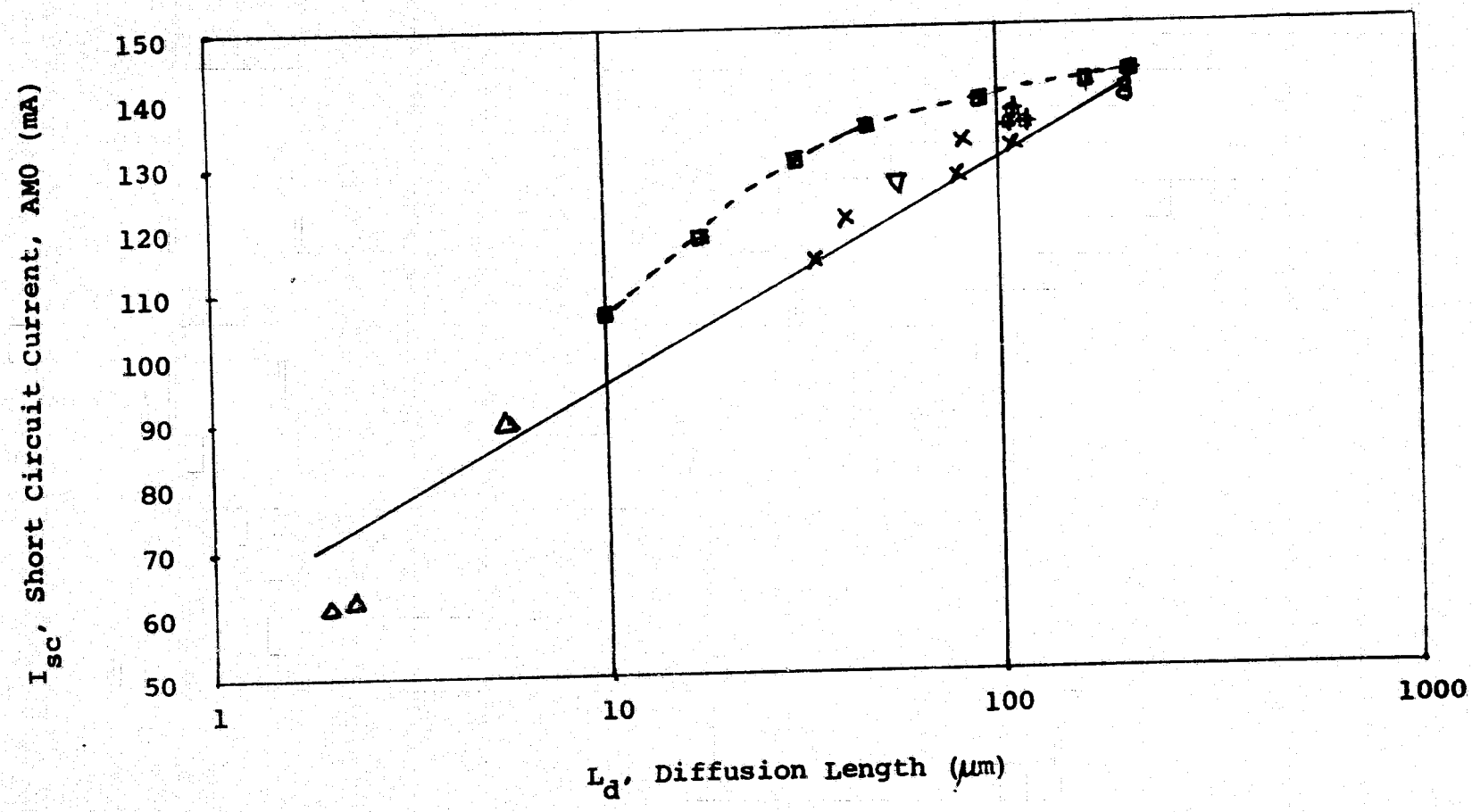

FIGURE 16

Spectral Response vs. Wavelength

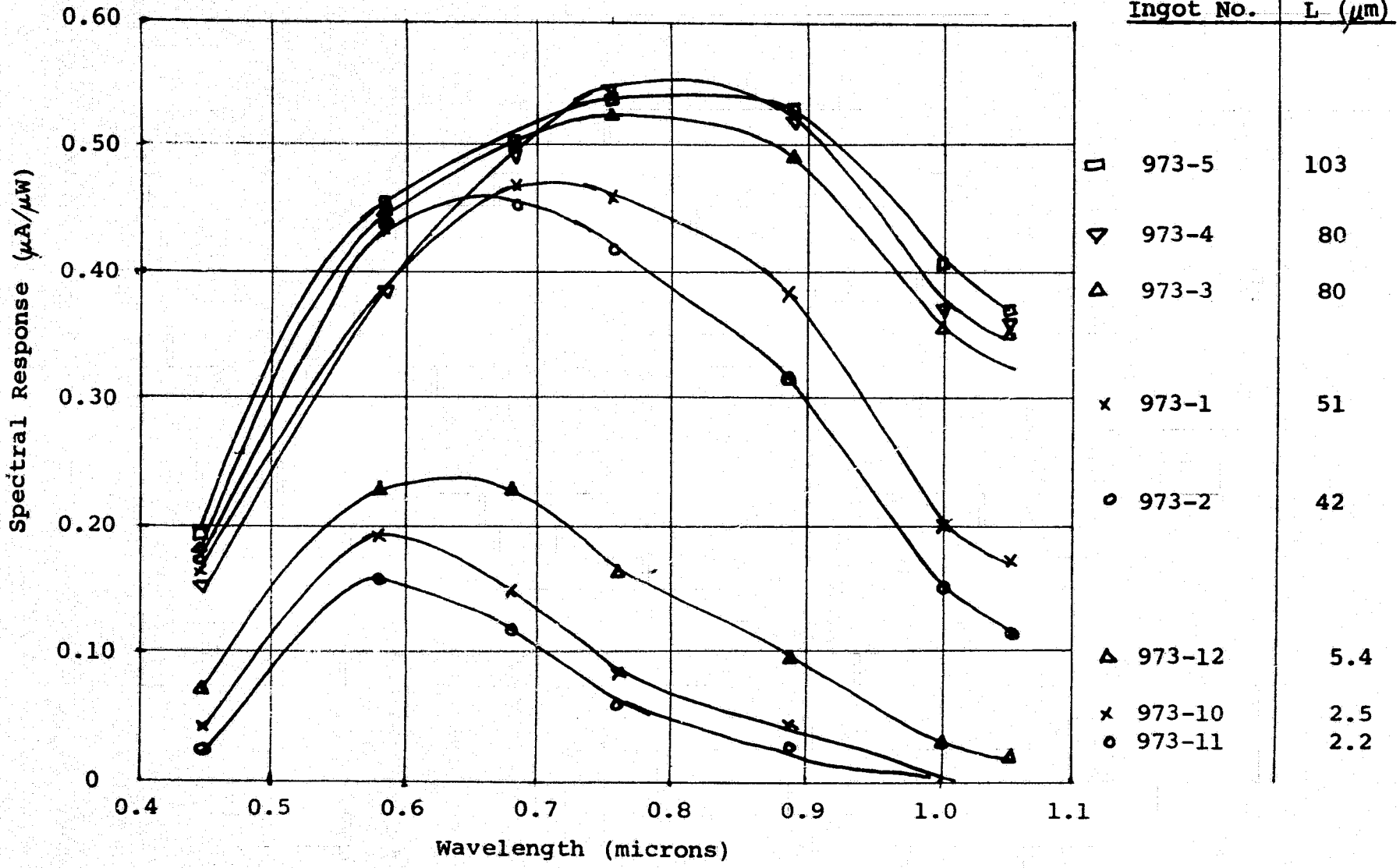

FIGURE 17

Spectral Response vs. Wavelength

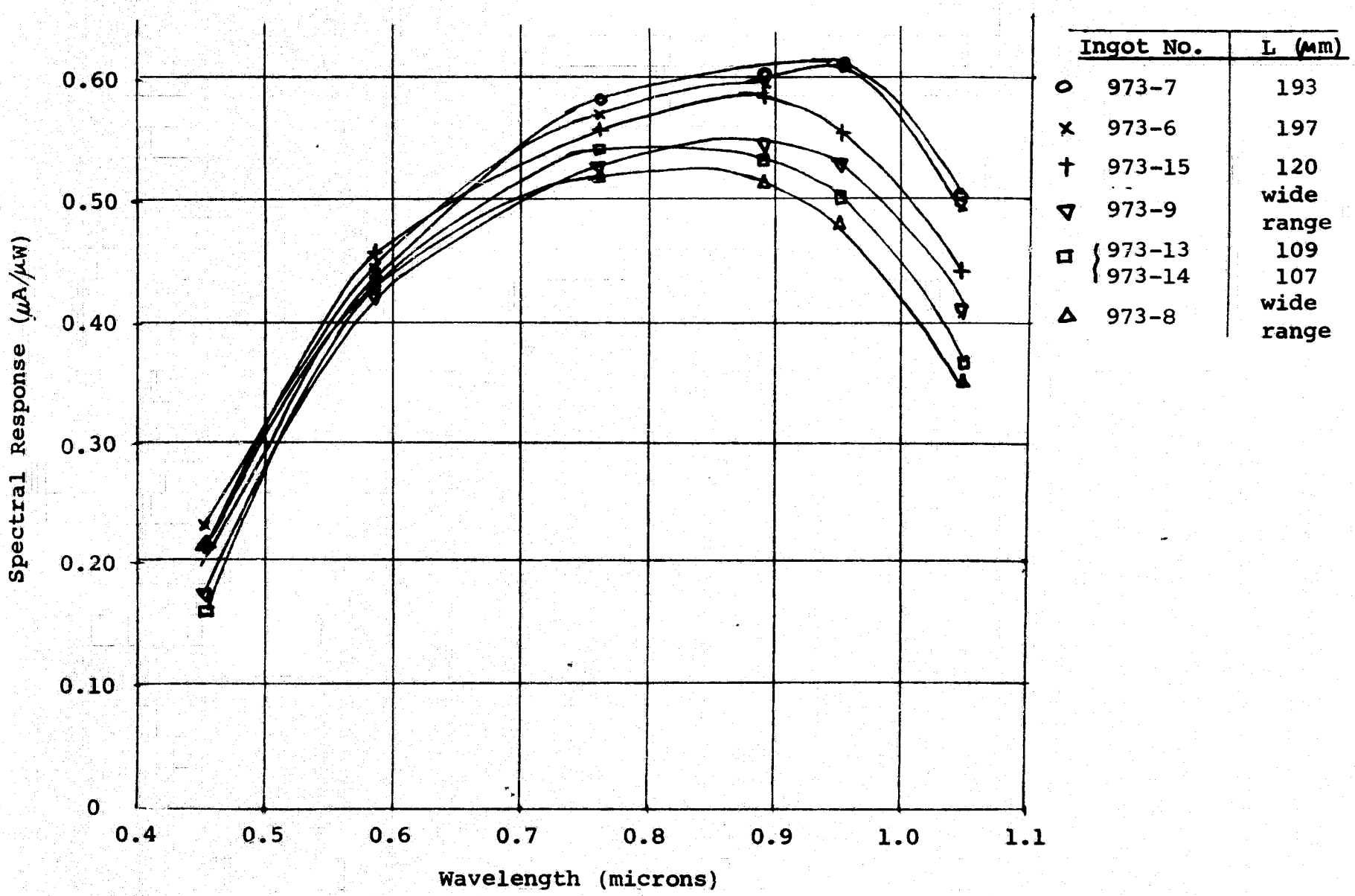

Ingot No.	L (μm)
973-7	193
973-6	197
973-15	120
973-9	wide range
973-13	109
973-14	107
973-8	wide range

FIGURE 18

Open Circuit Voltage vs. Acceptor Concentration

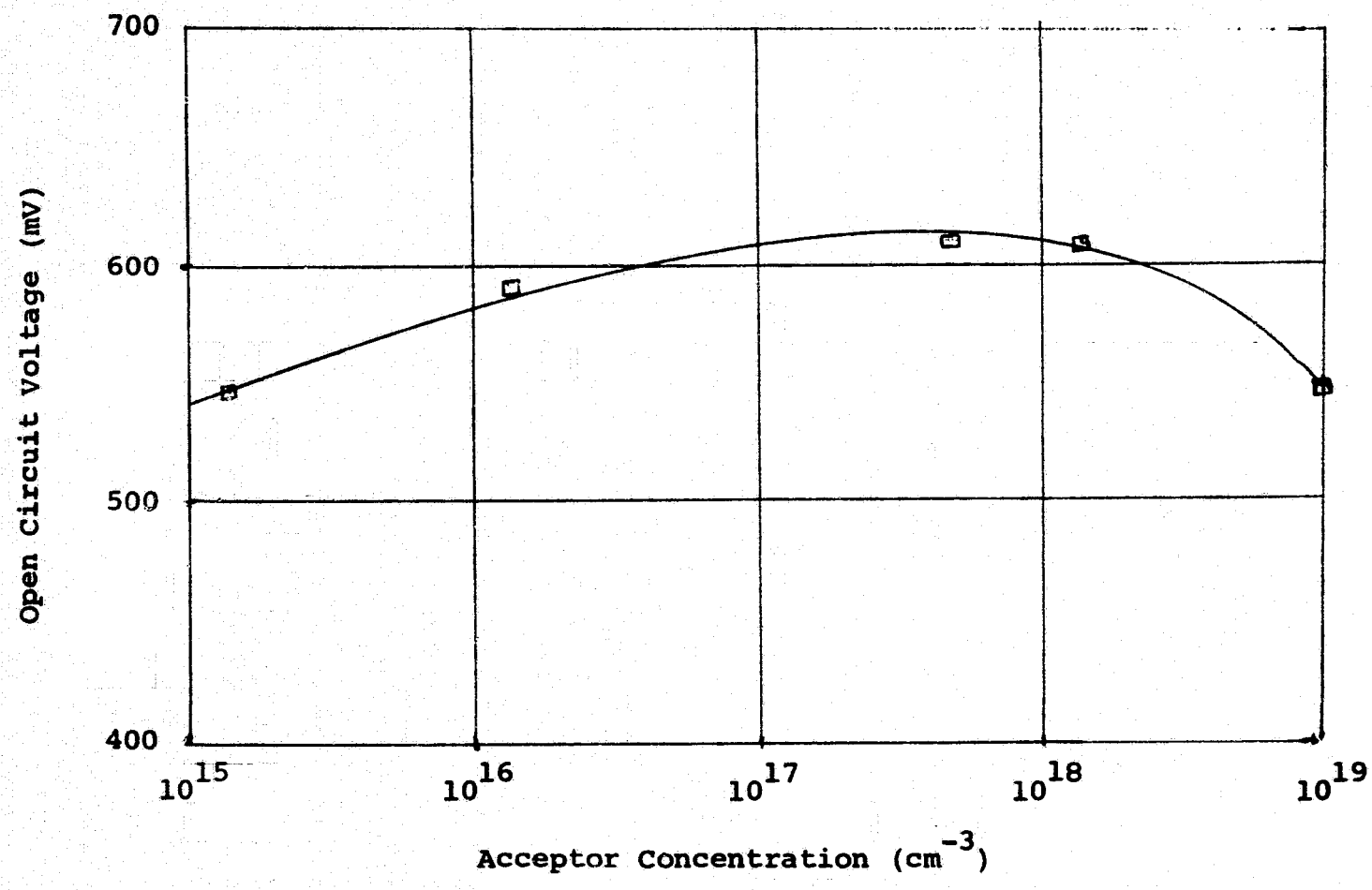

FIGURE 19

Forward Voltage Distribution on Mesas for Three Resistivities

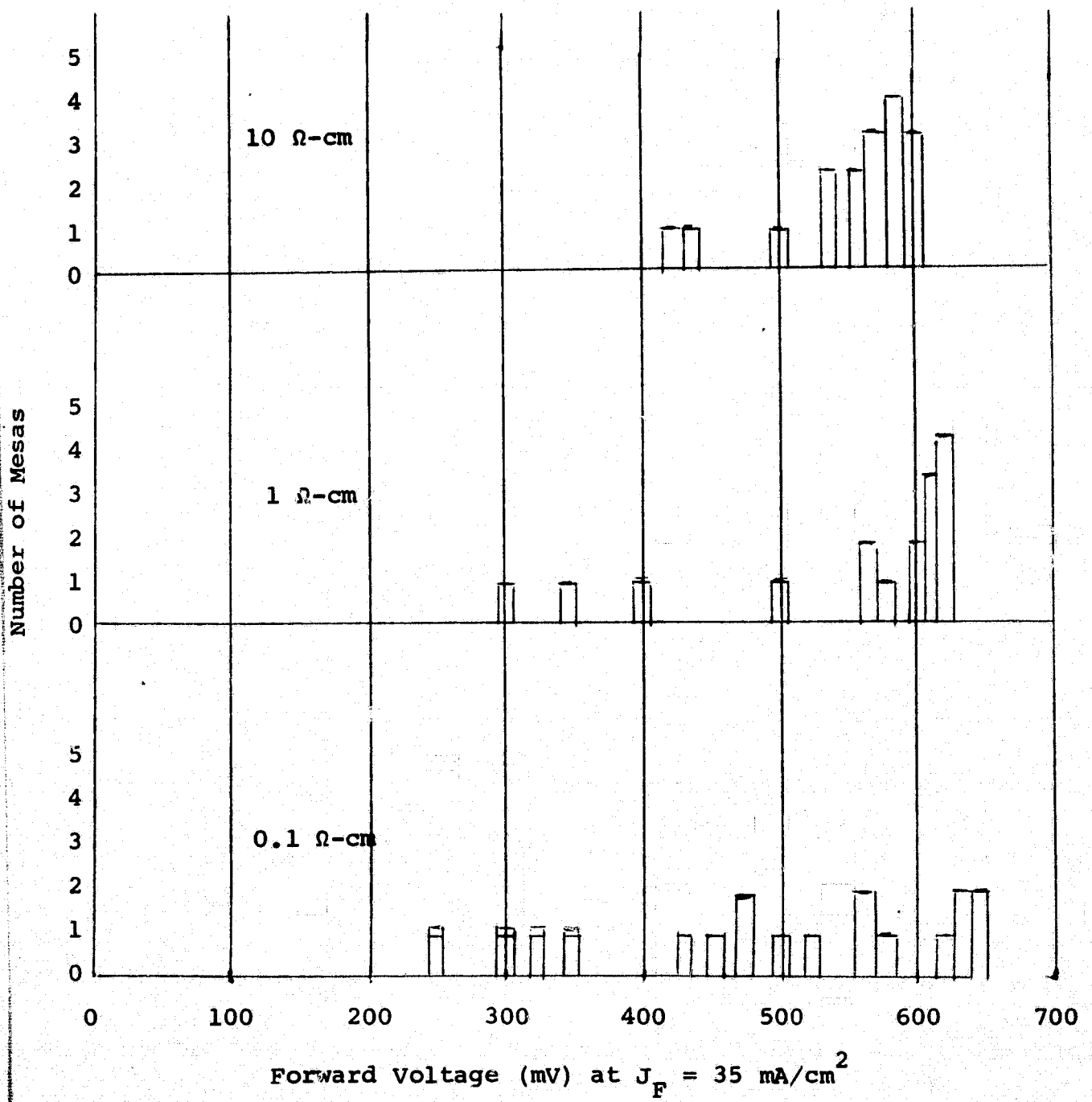

FIGURE 20

Envelopes for ln I_f vs. V_f for Three Resistivities

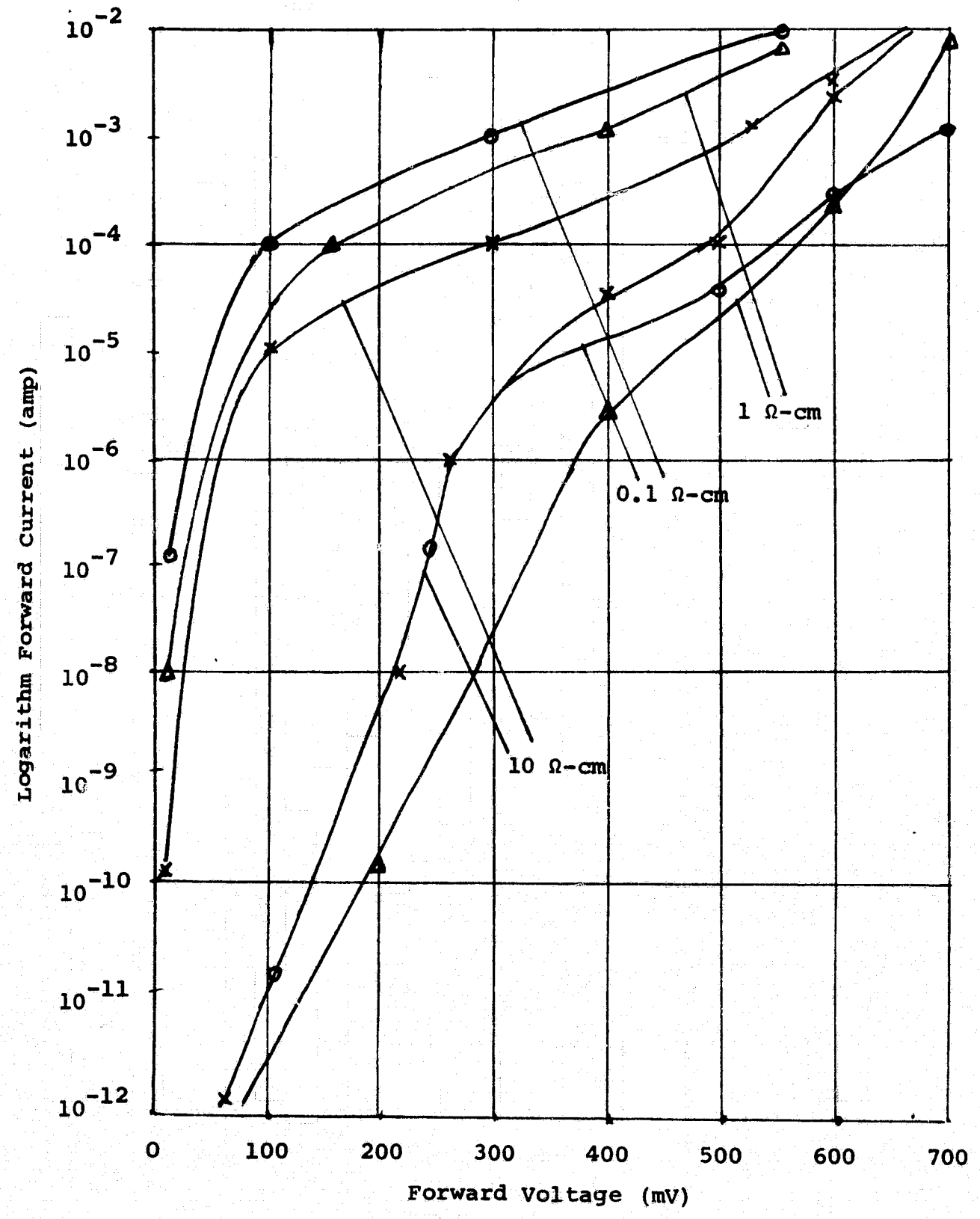

FIGURE 21

Envelopes of ln I_f vs. V_f for Three Junction Depths

Resistivity = 0.2 ohm-cm

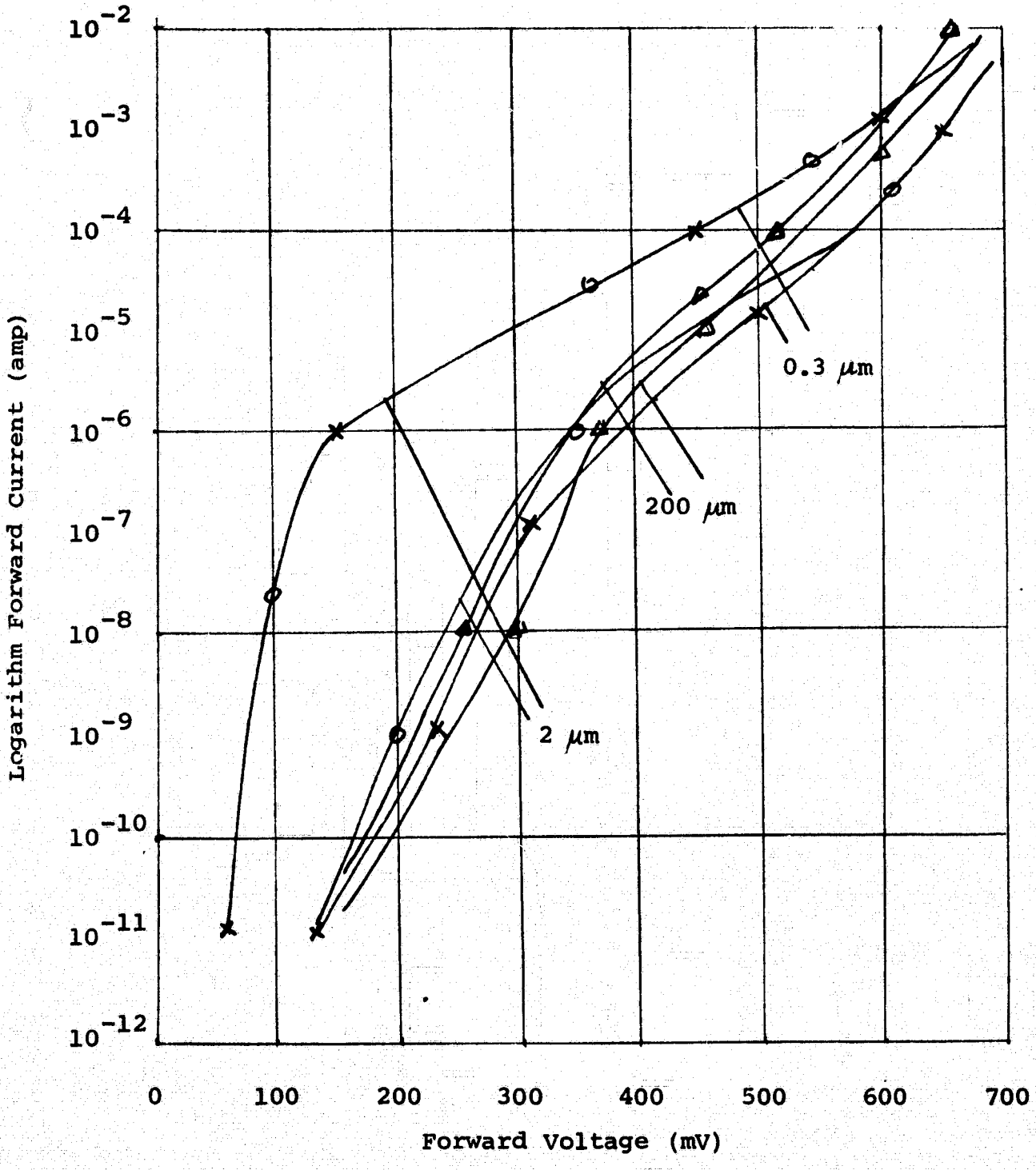

C-2

FIGURE 22

Envelopes of ln I_f vs. V_f for Three Junction Depths

Resistivity = 10 ohm-cm

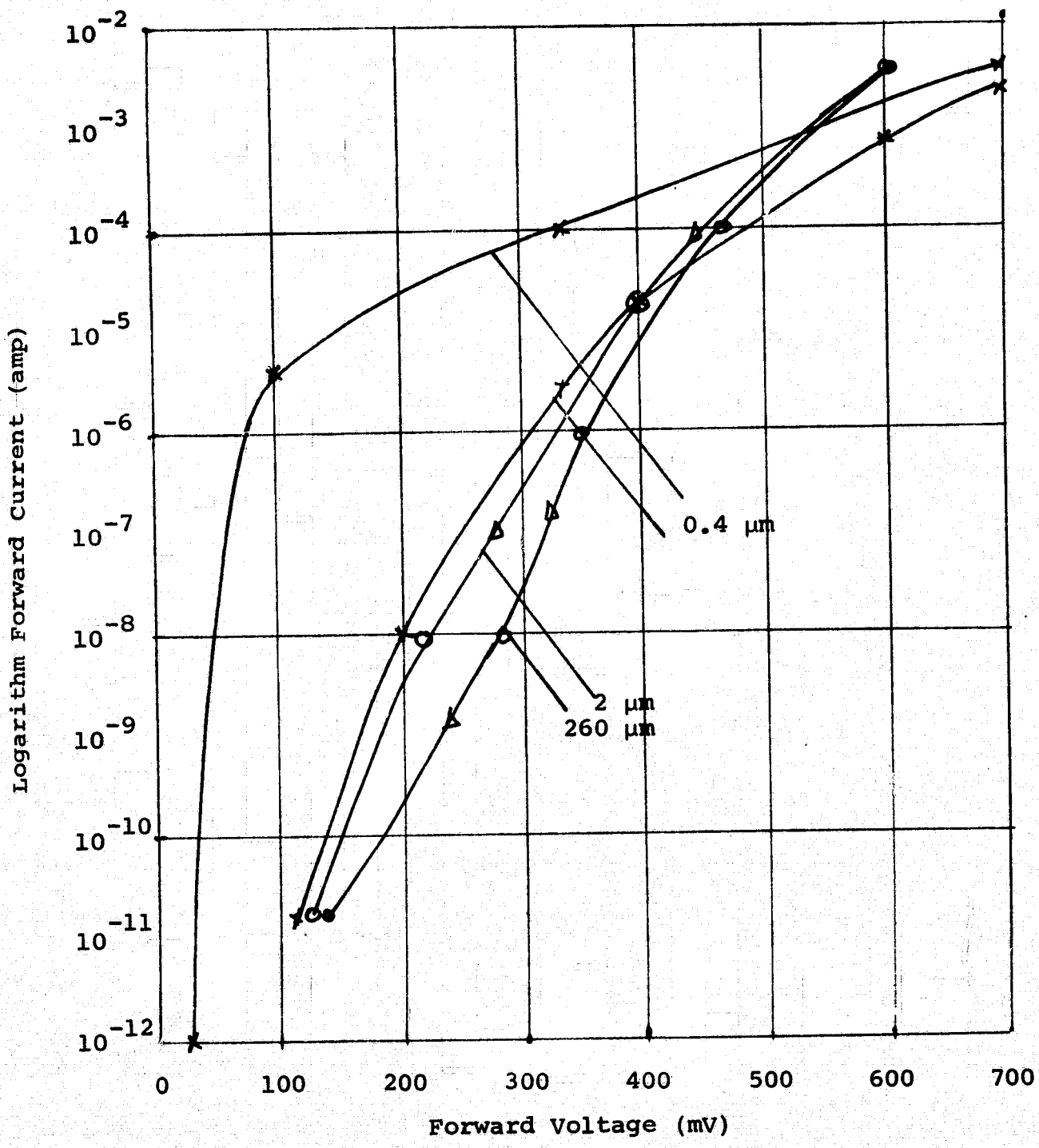

FIGURE 23

Open Circuit Voltage vs. Acceptor Concentration

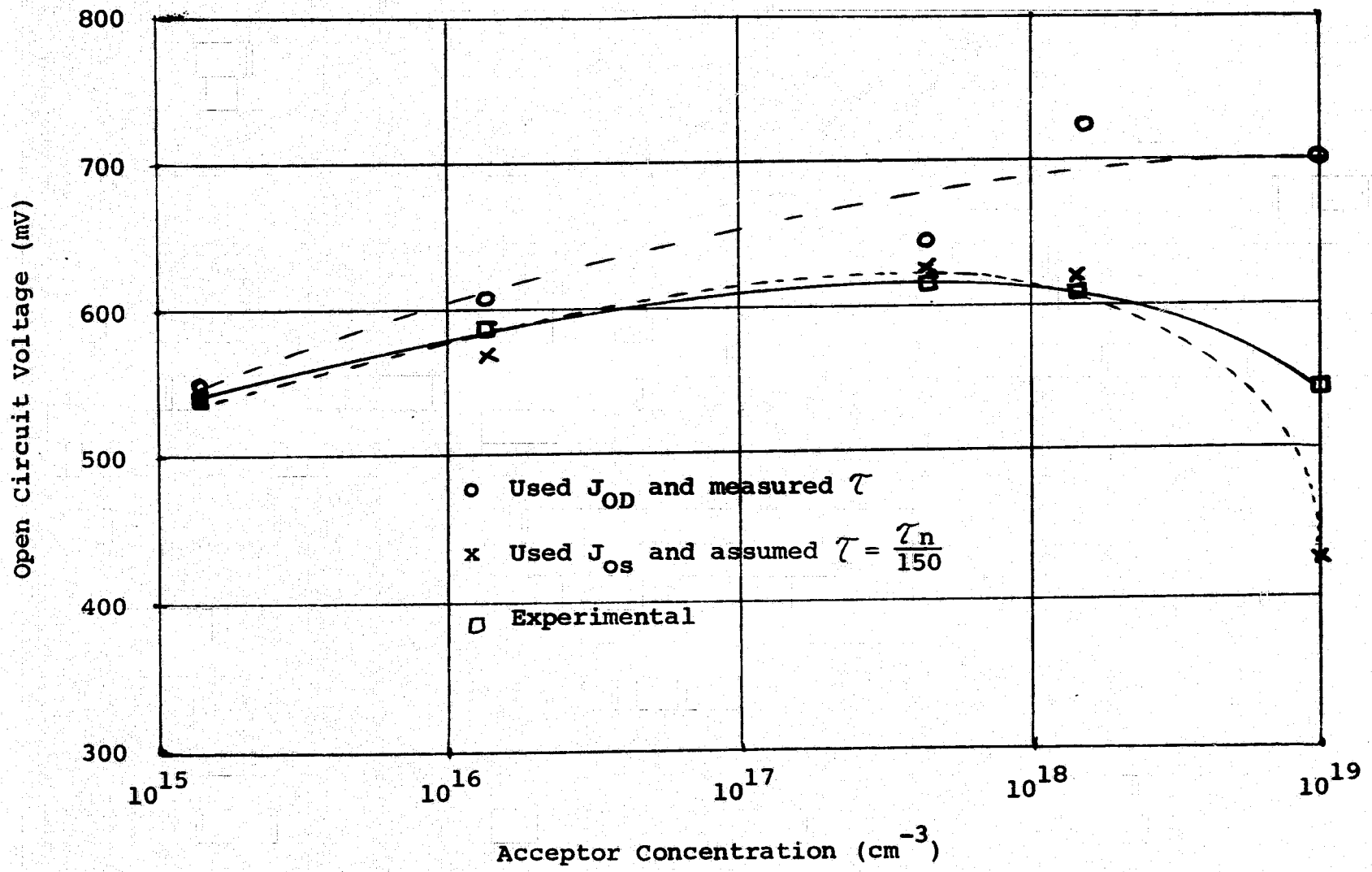

FIGURE 24

Geometric Arrangement for Theoretical Analysis

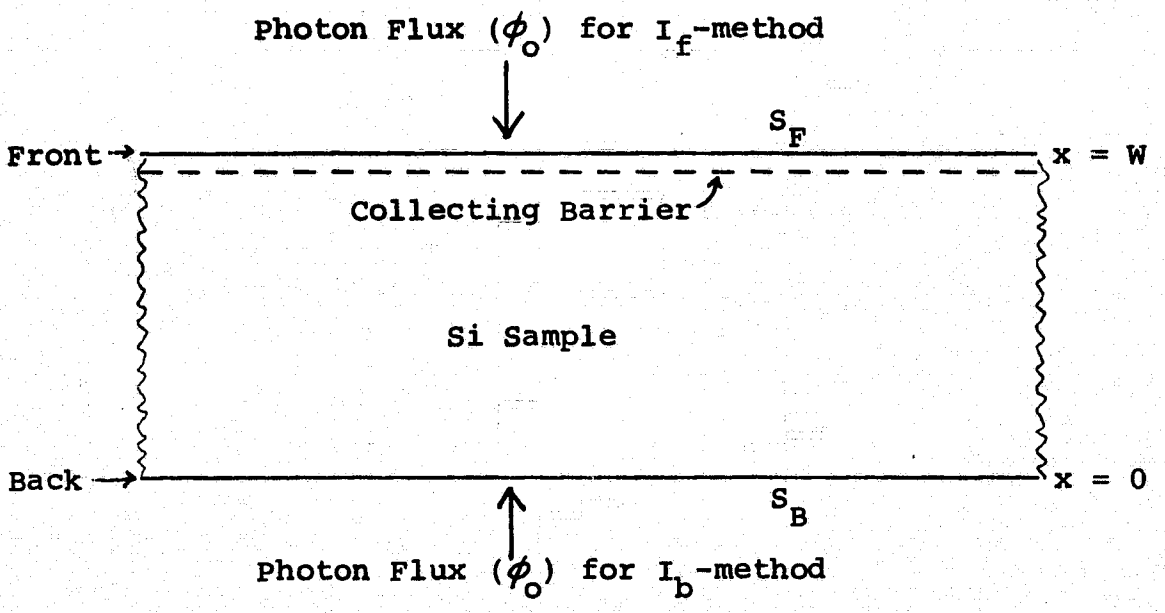

FIGURE 25

Later Measurement Circuit

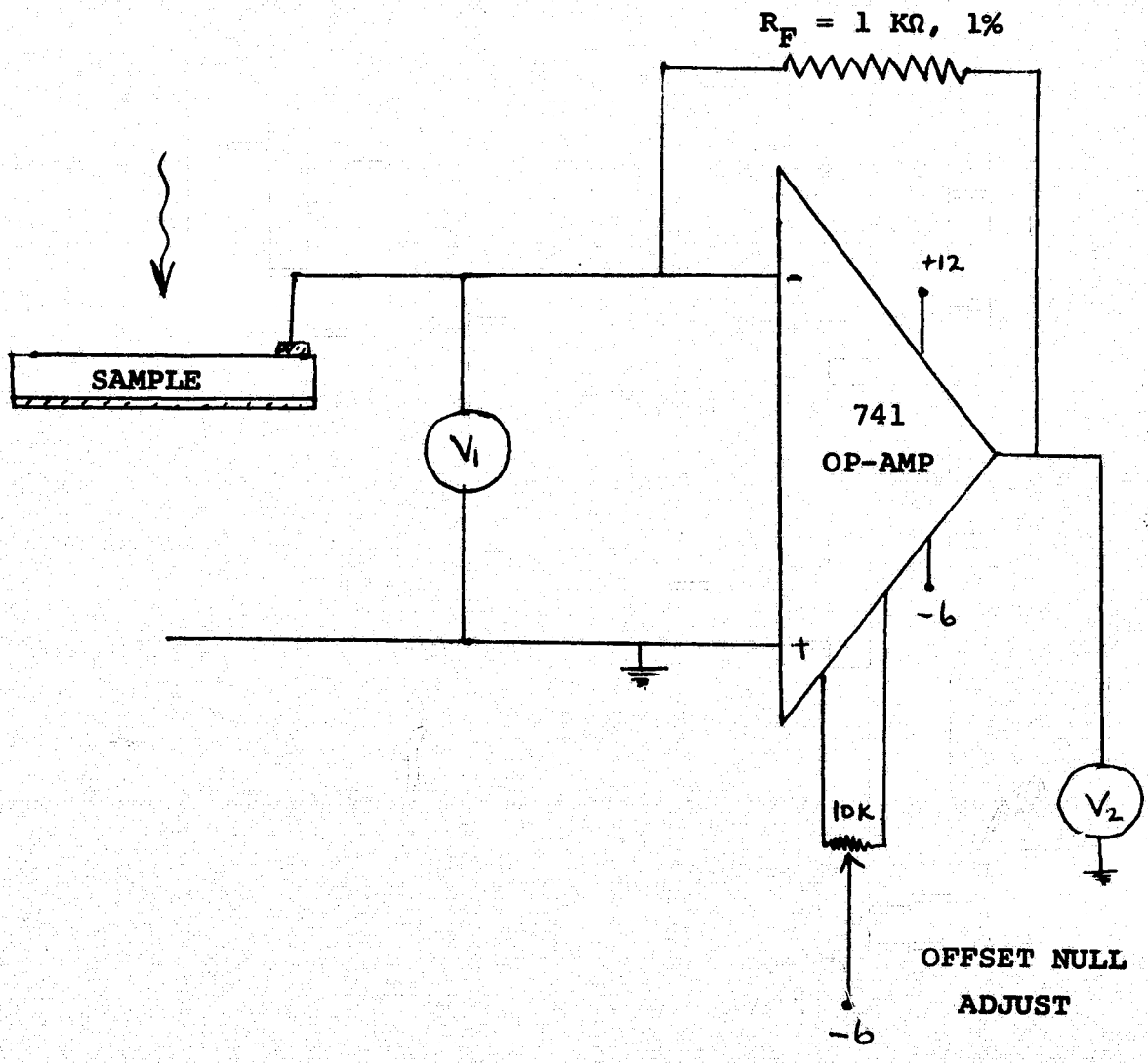

FIGURE 26

Front Current (Tungsten + 1.06 μm filter) vs. L_{EV}

$\alpha \sim 10.4\ cm^{-1}$

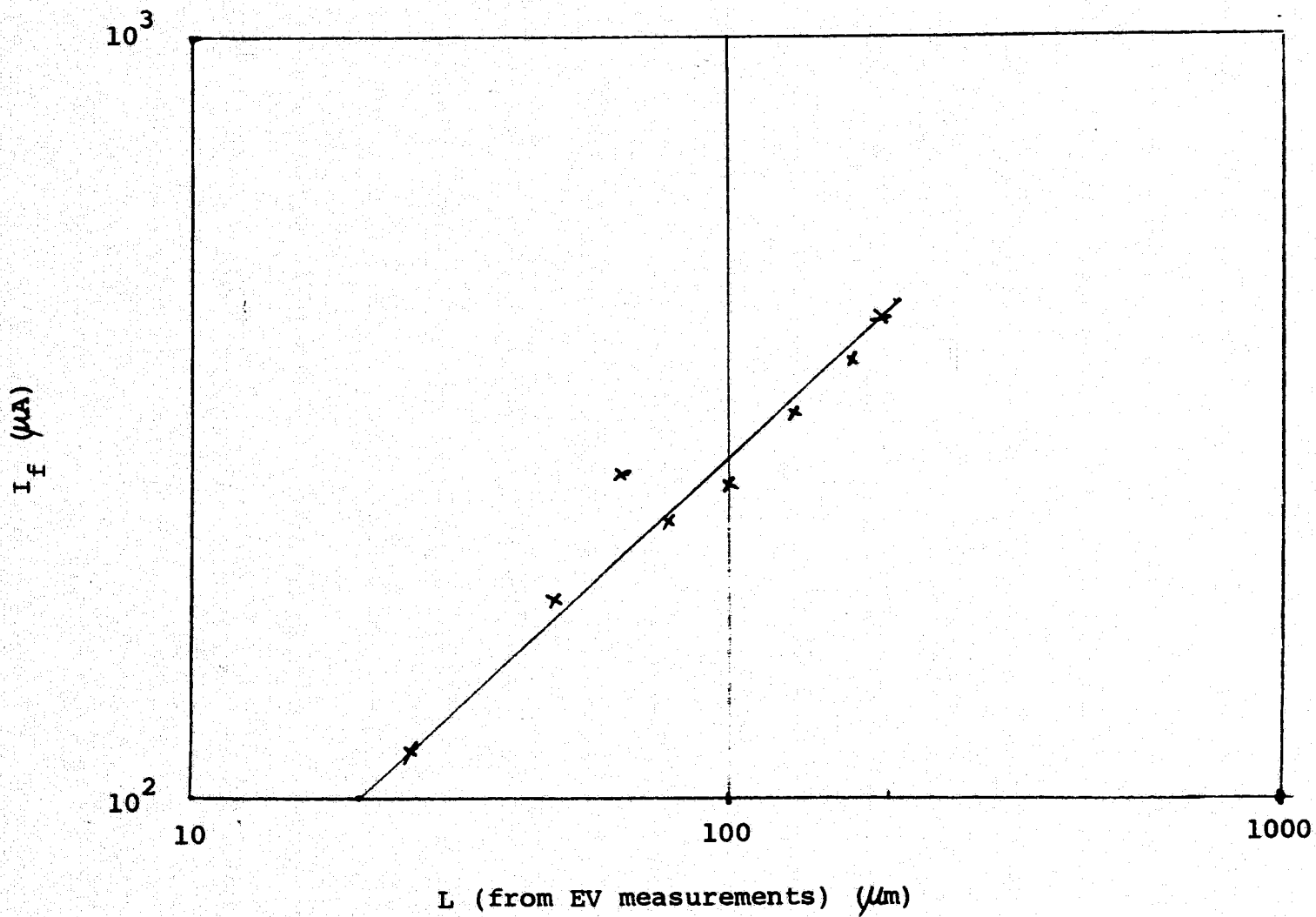

FIGURE 27

Absolute Spectral Response for Cell 2A-4B

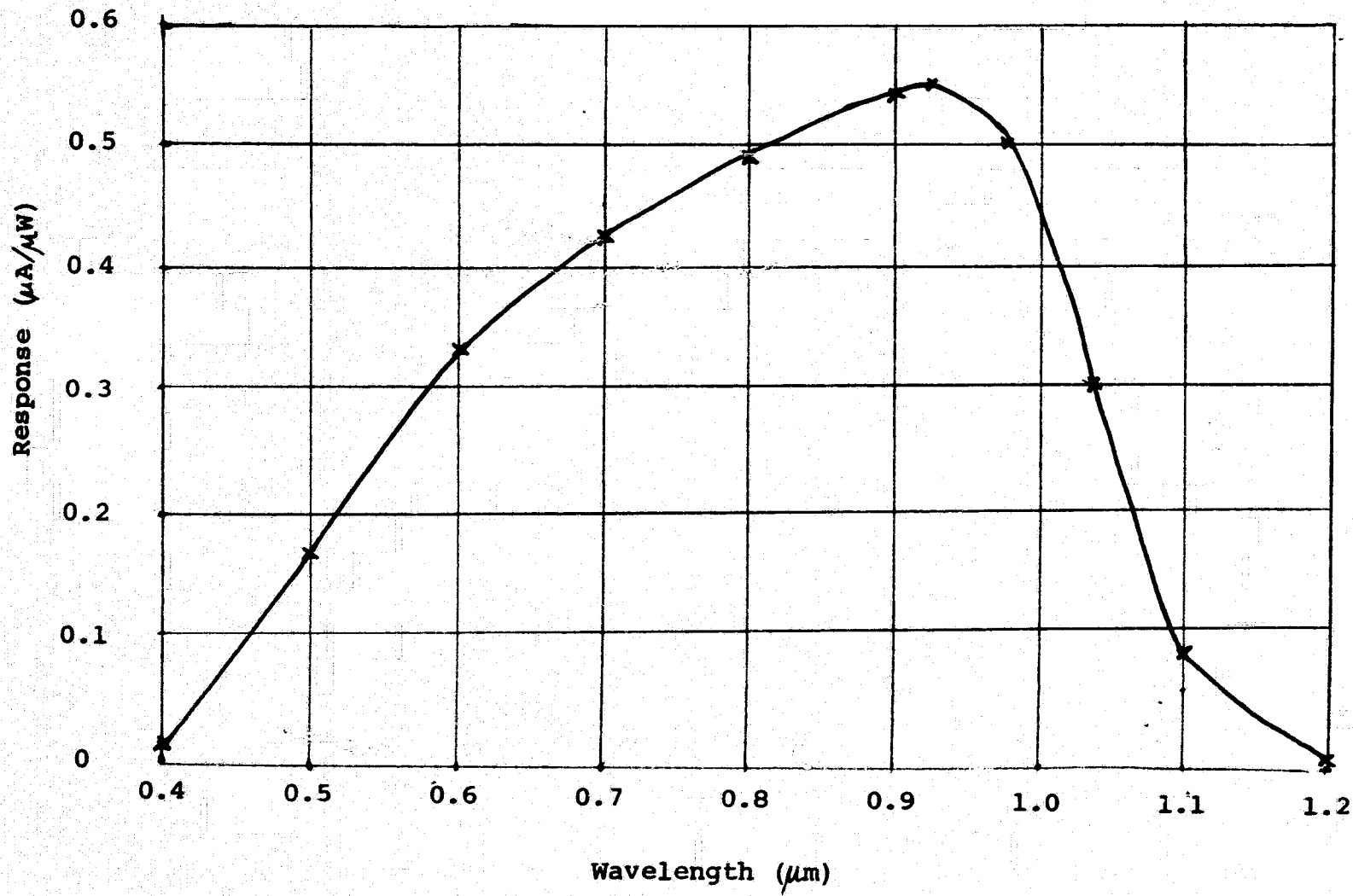

FIGURE 28

Step Sample

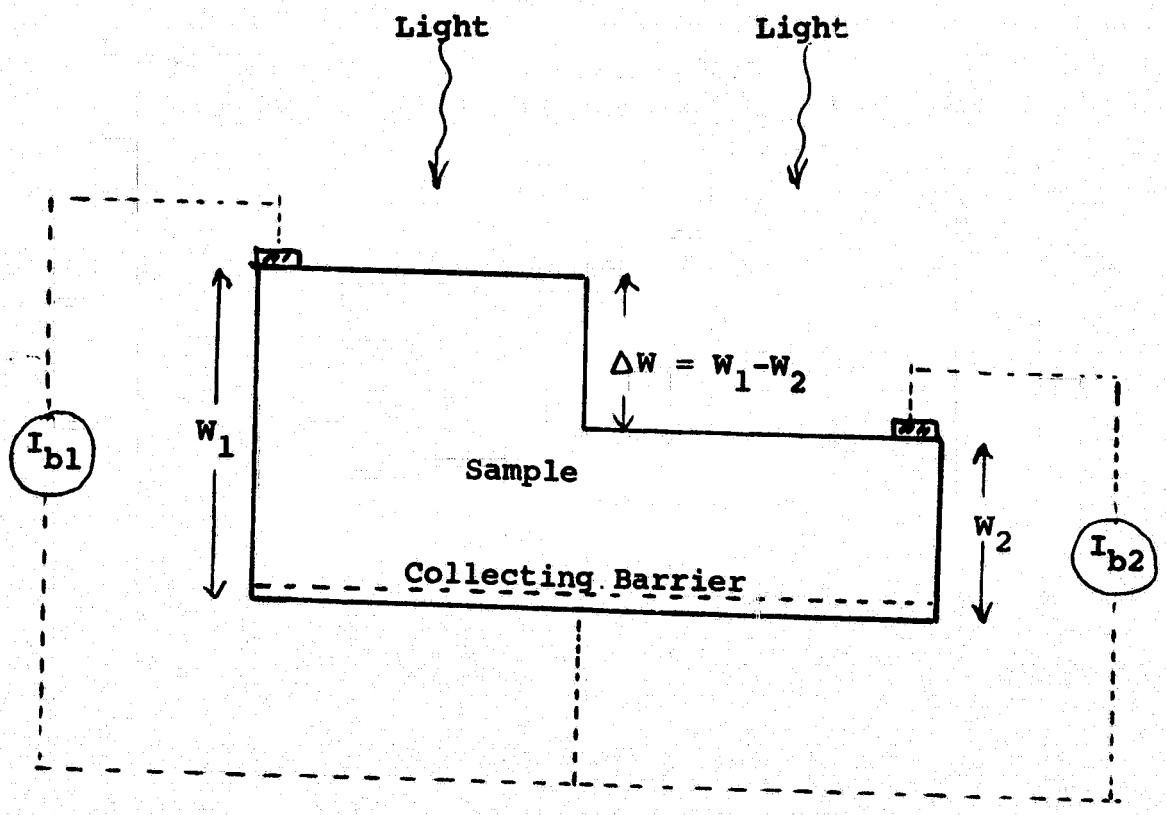

FIGURE 29

log (Back Current) vs. log (Slice Thickness)
for 973-9 (Long L-ingot)

LEGEND: x - undiffused samples
o - diffused samples

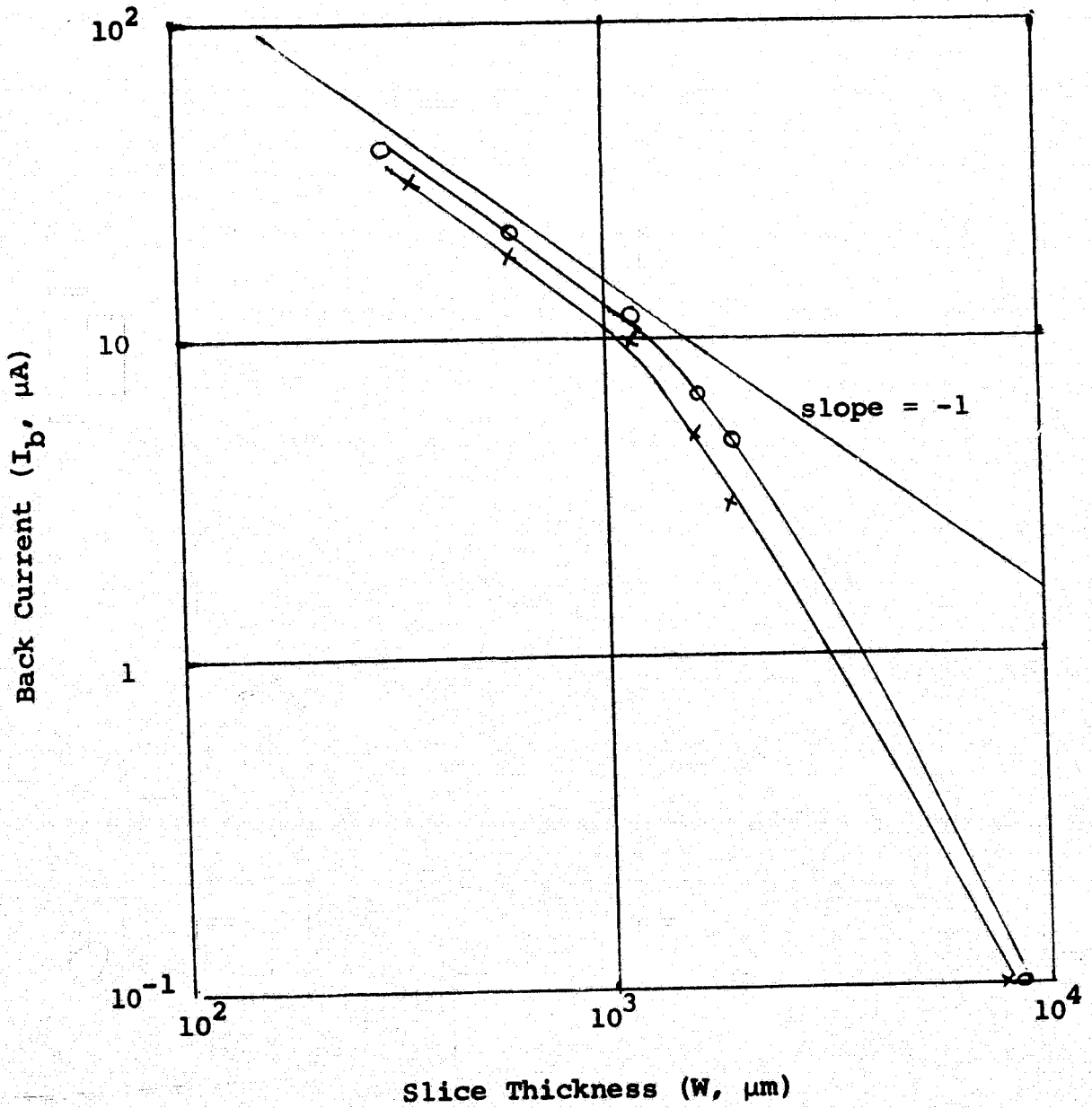

FIGURE 30

log (Back Current) vs. Slice Thickness

for 973-9 (Long L-ingot)

LEGEND: x - undiffused samples
o - diffused samples